Delayed response of low latitudes TEC during thirty-six geomagnetic storms from 2014 to 2017

Heba Salah Mohamed, Christine Amory-Mazaudier, Sampad Kumar Panda, O.M. Shalabiea, A. Mahrous

Delayed response of low latitudes TEC during thirty-six geomagnetic storms from 2014 to 2017

Heba Salah Mohamed[1,2,3], Christine Amory-Mazaudier[4], Sampad Kumar Panda[5], O. M. Shalabiea[2], A. Mahrous[6]

[1]Space Weather Monitoring Center, Helwan University, Cairo, Egypt
[2]Cairo University, Faculty of Science, Dept. of Astronomy, Space Science and Meteorology
[3]Canadian international college, Basic Science Department, Egypt-Japan University of Science and Technology
[4] Sorbonne Université, Ecole polytechnique, Institut Polytechnique de Paris, Université Paris
[5]Department of ECE, KL Deemed to be University, Koneru Lakshmaiah Education Foundation, Vaddeswaram, Guntur, Andhra Pradesh, 522303, India
[6]Saclay, Observatoire de Paris, CNRS, Laboratoire de Physique des Plasmas (LPP), 75005 Paris, France

Corresponding author: Mohamed Heba heba.salah@aucegypt.edu

Abstract

Ionospheric response to the onset of geomagnetic storms is an important aspect for developing models towards better understanding and prediction of ionospheric parameters, particularly over the equatorial and low latitude sectors that are associated with several complexities. Our paper discusses the time response of the ionosphere (Δt_{iono}), where Δt_{iono} is the time elapsed from the onset of sudden storm commencement (SSC) of a magnetic storm to the absolute maximum value of DVTEC (TEC: total electron content). Over the period 2014 to 2017, thirty-six storms are reviewed, and their Δt_{iono} are analyzed along with the magnetic and solar parameters. We defined a threshold value of TEC to be 8 TECU. Three storms are studied in detail as a reference for the entire range of storms (March 2015, June 2015, and September 2015). The stations used are Kourou (KOUR; 5.25°N/52.80°W) in the American longitude sector, Addis Ababa (AAE; 9.03N°/38.76°E) in the African longitude, Port Blair (PBRI; 11.63°N/92.71°E) and Patumwan (CUSV; 13.73°N/100.53°E) in the Asian longitude sector. In the Asian and American sectors, for all storms combined, there is no significant correlation (0.44 for the Asian sector and 0.22 for the American sector) between the delay (SSC time/time of maximum DVTEC) and the minimum of the Dst as found by previous studies. Instead, we considered geomagnetic storms satisfying the criteria: a) SSC occurs on the day side, and b) the origin of the magnetic storm on the solar disk must be far from the limb or does not belong to the far side, to obtain a much better correlation. The highest correlation value is observed at Thailand (0.84), followed by India (0.79) and South America (0.759), and the minimum value at Africa (0.641). The average response time in our study was found to be about 27.2 hours. We observed positive and negative ionospheric storms, five negative storms in South America

followed by two in Asia and a single negative storm in Africa from which it is realized that the most negative storms are in the time range of 9-15 LT. Nevertheless, there is hardly any relationship between the strength of DVTEC amplitude and the intensity of magnetic storms irrespective of longitude sectors.

Keywords: *Geomagnetic storm; Sudden Storm Commencement; Total Electron Content; Ionospheric response time; Equatorial region.*

1. Introduction

Geomagnetic disturbances are primarily caused by the magnetic reconnection that establishes an electrodynamical coupling between the solar wind plasma and the earth's magnetosphere. It is well known that the primary cause of geomagnetic storms is a strong dawn-to-dusk electric field associated with the intense and long duration southward turning of interplanetary magnetic field (IMF-Bz) (**Gonzalez et al.,1994**). When Bz is strongly negative, the magnetic reconnection between the IMF and the geomagnetic field produces open field lines that transfer mass, energy, and momentum from the solar wind to the magnetosphere **(Davis et al., 1997)**. The deposition of solar wind energy in the magnetospheric polar cap region causes a disturbance in the geomagnetic field. Geomagnetic storms produce significant and rapid changes in magnetospheric convection currents **(Chakraborty et al., 2015**). Intense storms are those with a peak disturbance storm time index (Dst) of -100 nT or less, moderate storms fall between -50 nT and -100 nT, and weak storms are those between -30 nT and -50 nT (**Gonzalez et al.,1994**). Because of this disturbance, the energy inputs from the magnetosphere to the upper atmosphere can cause a dramatic change in the electron density of the F region of the ionosphere. During the magnetic storm, intense joule and particle heating cause a strong upwelling of the atoms around the auroral oval. The strong upwelling transports oxygen or rich nitrogen up from the thermosphere to the F region; the neutral wind redistributes oxygen and rich nitrogen over high and mid-latitudes. Atomic oxygen, the principal constituent in the height range, shows a complex behaviour with a moderate increase and decrease in density at higher and lower altitudes, respectively. This indicates the height-dependent behaviour of the atomic oxygen, thereby affecting the vertical distribution of ionospheric densities. Earlier studies of ionospheric storms reveal a change from a positive to negative disturbance effect at mid-latitude with the enhanced intensity of a magnetic perturbation (Appleton & Naismith, 1935). During the storm, the Joule heating and particle precipitation at the auroral region causes the meridional neutral wind to transport air with depleted oxygen atoms [O] and enriched neutral nitrogen molecules [N2] equatorward and deposit across the middle to low latitudes. This results in the

enhancement of [O/N2] ratio in the equatorial region and its depletion in the polar regions, manifesting a reduced Total Electron Content (TEC) in middle to low-latitude regions. The transport of [O/N2] is vital at post-midnight hours owing to wind surges from ion convection and the associated movement transfer to neutrals. With sufficient wind surges [strong], the distributed region extends to the middle or low latitude and then coronates with the earth. At sub-auroral latitudes, depletion occurs shortly after a magnetic storm due to Joule and particle heating in the nearby aurora oval. In contrast, the low latitude penetrating depletion observed with a few hours delay after a magnetic storm is due to the subsequent equatorward mass transport from the night side auroral oval **(Zhang, 2004).** There are two explanations for negative ionospheric storms which may occur solely or conjointly: a) The increase in plasma temperature observed during ionospheric storms **(Evans, 1965; Prölss, 1976a)** compensates for the decrease in plasma density in the topside ionosphere and b) The coupling between the [O/N2] concentration ratio and the plasma density is local time-dependent. The negative ionospheric storms are determined mainly by the perturbations in neutral composition irrespective of solar activity conditions though the effects of vibrationally excited molecular nitrogen and oxygen cannot be neglected during high solar activity periods. In general, positive storms prefer to develop on the dayside when the contributions from the penetration electric field are more important. However, the negative storms are highly responsive to the early morning sector when the contributions from the disturbance dynamo electric field and the penetration electric field are comparable on the nightside.

Local time changes are essential to the coupling between the neutral and the ionised atmosphere, and this becomes obvious for nighttime conditions when the plasma density is determined primarily by loss and transport processes but not by the photoionization production. These include systematic changes with disturbance intensity, magnetic position, local time, and the season. A comparison is made between the longitudinal variation of [O/N2] density ratio and the longitudinal variation of magnetic invariant latitude along a constant geographic latitude, where all densities are adjusted to a common altitude. **Prölss, (1980)** found a good agreement between the systematic variations of both parameters, clearly demonstrating the invariant latitude control of compositional disturbances**.** Besides the geometric effect, there is also a modulation of the disturbance magnitude with more significant perturbations near the longitude of the geomagnetic pole (i.e., near 290 degrees east in the northern hemisphere and 110 E in the southern hemisphere). Although positive ionospheric storms have been earlier linked to the changes in the neutral composition **(Duncan, 1969; Obayashi, & Matuura, 1970)**, it is now

generally believed that positive ionospheric storms are mainly caused by the transport of ionisation. There is hardly any correlation between the positive ionospheric storm and changes in the neutral composition (Prölss, 1976b). It might be caused by ionisation transport, which is affected by winds and- or electric fields. Different studies investigated the ionospheric response in both High-Speed Solar Streams (HSSs) and High-Intensity Long-Duration Continuous Auroral Electroject Activities (HILCDAA) during 2008–2009 **(De Siqueira Negreti et al., 2017; Koga et al., 2011; Sobral et al., 2006; Tsurutani et al., 2004; Wei et al., 2008)**. In this context, the time delay is considered to be an important feature of the associated ionospheric storm that refers to the time interval between the onset of the Sudden Storm Commencement (SSC) or main phase onset (MPO) of magnetic storms and the time of maximum ionospheric response. **Balan & RAO, (1990)** reviewed the delay between SSC onset and the ionospheric responses for positive and negative storms at mid and low latitudes using data for 60 geomagnetic storms with SSC occurring from 1968 to 1972 in North America. They used storm time deviation DVTEC, itis calculated from a monthly median (VTEC). Their analysis demonstrates that for daytime SSCs, the time delays are low for positive responses and high for negative responses with opposite signatures for nighttime SSCs. However, concerning the intensity of the storms, the time delays are inversely proportional to the level of intensity in their study.

Liu et al., (2014) studied TEC response to geomagnetic storms during the 14-17 July 2012 and reported the reoccurrence of a negative ionospheric phase with a delay of about 24 hours. **Jimoh et al., (2016)** investigated the TEC response during two equatorial storm events in 2012 and confirmed a temporal response of more than 24 hours. **Cander, (2016)** examined 15 major storms in solar cycle 24 at mid-latitude stations with storm time TEC differences from monthly median level and found that thermosphere winds and electric fields are the main drivers of ionosphere storms producing electron density changes beyond a climatological level. **Zolesi & Cander, (2014)** considered an ionospheric storm if the relative deviation ΔVTEC exceeds 25% for more than three hours. Their analysis shows that the strength of the positive/negative phases of the storms is correlated with the intensity of the geomagnetic storms. Further, VTEC amplitude tends to increase during the first 24 h of the geomagnetic storm (the positive phase) and then decrease below its quiettime baseline (the negative phase), followed by a recovery phase lasting for one or two days longer. On average, during ionospheric storms, there are a considerable number of positive phases followed by negative ones and an insignificant number of negative storms followed by positive ones **(Zolesi & Cander, 2014)**. The time delay of the

maximum positive VTEC deviation from the SSC time (PPSn) is 6 h. The time delay of the maximum negative VTEC deviation from the minimum Dst value NPM was 16 h (Cander, 2016). The negative phase becomes intense with increasing latitude whereas the positive phase lasts longer and is more prominent with decreasing latitude.**Iyer & Mahajan, (2021)** investigated the geomagnetic storms during 2015 to obtain the relationship between the deviation in storm time VTEC from monthly median values (DVTEC), aroral electrojet (AE) and Dst. Their results show that TEC and the considered geomagnetic indices (AE and Dst) do not establish a simultaneous relationship whereas the individual parameters are solely presenting certain relationship with DTEC. Aa et al., (2021) studied the the ionospheric response to a low-latitude annular solar eclipse event on 21 June 2020 at both eclipse and conjugate regions. They investigated both the large scale ionospheric variation and small scale perturbations induced by the solar eclipse. The DTEC calculation is deduced by subtracting the average TEC values of the reference 10-quiet days from the eclipse day. They found TEC depletion in the Asian sector with a slightly different longitudinal and altitudinal response during the eclipse.

It is realized from the past reports that the time delay between a magnetic disturbance and the associated atmospheric perturbation is a key parameter in studying the geomagnetic activity effect. However, there are hardly any studies on statistical analysis on ionospheric response time to the onset of geomagnetic storms of different intensities over the equatorial and low latitude regions, particularly during the previous solar cycle (solar cycle 24). Also, it is not clear about the association between storm time and ionospheric responses that manifests diverse relationship between the ionospheric, solar and geomagnetic parameters. Hence, in the present work, we aim to survey the geomagnetic storms during the declining phase of solar cycle 24, taking into consideration of the solar and magnetic indices, and statistically evaluating their response time (Δt_{iono}) at four equatorial locations corresponding to three longitude sectors during the period from 2014 to 2017. In brief, we take into account the position of the source of the disturbance on the Sun and the occurrence time of the SSC as the two main criteria for selecting the events considered in this study. The storms with different intensities, sources are included in the correlation. A linear relationship between the Dst index and Δt_{iono} in the ionosphere is derived by emphasizing the mximum absolute DVTEC during the storm. The refining criteria chosen in this work has established a more reliable correlation between the Dst and Δt_{iono} to deduce a mathematical equation, which has been the major focus of this study. The paper is organised as follows: section 2 presents the data sets methodology adopted in this work.

The section 3 represents the results obtained during three significant storms and the generalization of storm time effects. The discussions of the results are presented in section 4, followed by the concluding remarks in section 5 of this study.

2. Data and Methodology

In the present work, we considered the geomagnetic storms during the solar maximum and descending phase of the 24th solar cycle comprising the period from 2014 to 2017. The list of geomagnetic storms can be accessed from Observatori de l'Ebre website (http://www.obsebre.es/) and the corresponding magnetic indices used in this research were obtained from International Service of Geomagnetic Indices archives (http://isgi.unistra.fr/). Solar indices were obtained from the Space Physics Data Facility (SPDF) archive (https://spdf.gsfc.nasa.gov/data_orbits.html). To characterize the geomagnetic storms and their different phases, we used the planetary K index (Kp) and Disturbance Storm Time indices (Dst). The AE index is considered to indicate the high latitude geomagnetic activity morphology. We also used the solar wind speed (V_{sw}) and southward pointing interplanetary magnetic field (IMF-Bz) component in GSE coordinates, downloaded from the Omni website (https://omniweb.gsfc.nasa.gov). The solar disk phenomena and events are observed using the Solarham website (http://www.solarham.net).

The equatorial TEC values were derived from dual-frequency GPS observations at four international GNSS service (IGS) stations around the magnetic equator during the period from 2014 to 2017. The GPS station code, location and geographic as well as geomagnetic coordinates of the stations are presented in Table 1 and the geographic locations of stations on the global map are shown in Figure 1. The GPS observations files are routinely provided by the IGS at the CDDIS-NASA archive (ftp://cddis.gsfc.nasa.gov/). The world data centre for Geomagnetism (WDC, Kyoto) runs the IGRF model to provide the corresponding geomagnetic coordinates for any geographic coordinates which can be accessed from its website (https://wdc.kugi.kyoto-u.ac.jp/igrf/gggm/). Table 2 shows the SSC date and time and corresponding Dst minimum, maximum Kp index and solar origin of the 36-magnetic storms. It can be observed from the table that most of the storms are due to CME except for **6** events which are due to HSSW flowing from the coronal holes and occurred during 2017, corresponding to the declining phase of the solar cycle 24. In Tables 3 and 6, we present the

ionospheric response delay characteristics at the African (AAE) and South American (KOUR) equatorial stations whereas in Figures 4 and 5, the response delay characteristics at the two Asian stations (PBRI and CUSV) are presented.

A detailed description of the general procedure used to analyze the ionospheric response time in this study can be obtained from earlier literature **(Balan & RAO, 1990; Liu et al., 2010)**. The storms considered in this study occurred during the maximum and declining phases of the solar cycle 24. We can see in Table 2 that there is a variety in the strength of the geomagnetic storms. However, they have a noticeable effect on the ionosphere; see Tables 3 to 6 in the 5^{th} column. During the geomagnetic storm, the difference in vertical TEC variability (ΔVTEC) is obtained by subtracting the median of the VTEC observed during the first five magnetically quietest days (QVTEC) from the VTEC variation on the storm day (VTEC). Consideration of median values from 5 most quiet days of the month may contain minor biases owing to the day to day variability. However, the bias limit remains below the range of storm time variations and is disregarded in the present study as the main aim is to find the time of highest deviation rather than epoch wise variations. There are several articles those consider average or median of first five quiet days as reference values for the storm time comparisons or model performance analysis (Balan & RAO, 1990; Iyer & Mahajan, 2021; Odeyemi et al., 2018; Silwal et al., 2021).

Further, we calculate the Δt_{iono} for each storm from the onset time of the SSC until the time of maximum ΔVTEC. The criteria we used to select the Δ VTEC (DVTEC) are as follows:

i. Firstly, the criteria to consider DVTEC (positive or negative) is its absolute value should be greater than 8 TECU. In our sample of 35 storms, only one storm has a data error. From the rest pf the storms, it is observed that the maximum value of DVTEC is 38 TECU, and the lowest value of DVTEC is 21% of this maximum value, i.e., 8 TECU. To minimize the uncertainty, we constrained the consideration of DVTEC which must not be less than 20% of the observed VTEC value.
ii. Secondly, we chose the delayed response to the storms during the recovery phase (after several hours), and for this period, we took the absolute maximum DVTEC and the corresponding time.

3. Results

3.1 Presentation of three storms

The absolute DVTEC and its respective maximum occurrence time during the recovery phase are calculated for three geomagnetic storms of different intensity levels. Figures 2a-2b refer to the most intense and first super geomagnetic storm in 24th solar cycle that occurred from March 17- 20, 2015. This magnetic storm occurred due to a CME associated with an X-class flare and a series of radio bursts around March 13th, 2015. **Nava et al., (2016)** analysed the characteristic effects of this storm in detail, and there is a special collection on this particular event in JGR. Figure 2a comprises four panels: from top to bottom, the Bz component of the Interplanetary Magnetic Field (IMF) in nT, the solar wind speed in km/s, the Kp index, and the AE magnetic index in nT. The Bz is positive and fluctuating until the morning of March 17th, it turns south and decreases to beyond - 20 nT on 17 March at 17:14 UT and keeps the same behavior until the end of the day. The primary causes of geomagnetic storms are strong dawn-to-dusk electric fields associated with the passage of south-oriented Bz for a sufficiently long interval in time **(Gonzalez et al., 1994)**. The solar wind speed increased on 17 March at 17:14 UT and continued to rise beyond 600 km/s until the end of March 20. The Kp is below 5 on March 16th and reaches a maximum value of 8 on March 17th, then decreases again on March 18-19. The AE index reaches the maximum of 1500 nT on March 17. In brief, Kp, AE and IMF show an enhancement on March 17, while the velocity has an enhancement on March 17-18. The vertical black line in each panel indicates the SSC occurrence.

Figure 2b presents the ionospheric observations for three different stations along with the Dst index from March 17 - 20, 2015. The first panel is the Dst index, and the second panel is South America's Kourou (KOUR) station depicts the variation of VTEC in blue, the median VTEC in red, and the DVTEC in black. The first vertical black line indicates the SSC time at 4:45 UT on March 17. The Dst index is a proxy representation of ring current variability that confirms the highest negative departure of -222 nT. The black point indicates the DVTEC maximum, with a value of 23.94 TEC occurring at 00:30 on March 18th. The VTEC and the median have the same values during the event except the interval from 00:00 to 12:00 on March 18th when a slight difference was noticed between the variables. The DVTEC shows small fluctuations during the event, except on March 18th at 00:30. We observed a negative DVTEC fluctuation at KOUR whereas the absolute value of these fluctuations is positive on March 18th at 00:30 UTC with a value of 23.94 TEC. The 3rd panel is for Adis Ababa (AAE) in Ethiopia. The VTEC and the VTEC median have almost the same values during the event, except on March 17 at

12:00 UT till late March 17. The maximum value of DVTEC is 33.14 TEC at 17:45 UT on March 17, similar to KOUR station; AAE DVTEC maximum is indicated with a black point and a label for coordinates (the time and the value for DVTEC) is indicated on the figure. The overall ionospheric fluctuations during the storm at this station were mainly positive. The 4th panel is for the CUSV station in Thailand, the SSC occurring at 04:45 UT is during the local daytime (LT). The VTEC is maximum with an amplitude of 83 TECU on 17 March 2015, at 14:30 UT. However, the DVTEC was negative on March 18 at around 10:00 UT with a value of 28.8 TECU indicated by a black point on the figure.

The geomagnetic storm occurring on 22-25, June 2015 is due to a CME and dual M-Flare event around region 2371 during the early hours of June 21st. **Kashcheyev et al., (2018**) studied this storm in detail. The storm's solar and magnetic parameters are shown in Figure 3a (similar to Figure 2a). The Bz component fluctuates slightly until early 22 June confirming a decrease in the amount of energy flow in the magnetosphere and a subsequent expansion during the main phase. The Bz value reaches a maximum negative value of - 40 nT in late June 22nd. The solar wind speed started at 300 km/s with a gradual increase until 700 km/s on late 22 June. The growth of the solar wind continues during the early morning hours on June 23rd, with a slight decrease at the end of 23 June with a further increase on 24 June. The Kp index started increasing from a level of 4 on 21 June to reach a value of 8 on 22 and 23 June and thereafter returning to the normal value of 3 on 24 June. The AE index shows a maximum magnitude of above 2000 nT at the end of 22 June and continued fluctuating until mid-June 23.

Figures 3b is similar to Figures 2b, for the storm of June 2015. The VTEC, DVTEC and median VTEC for the station KOUR (French Guiana) are shown in the 2nd panel in Figure 3b. The DVTEC is negative (-29.14 TECU) on 23 June 2015, at 18:45 UT, while the VTEC is 51.5 TECU on 22 June at 20:45 UT. The 3rd panel shows AAE station, where the storm was mainly negative and the DVTEC maximum occurred on June 23 at 07:00 UT with a value of -13.88 TECU. The 4th panel is PBRI, the DVTEC Maximum occur with 18.59 TECU on AAE on June 23 at 06:15. The behaviour of DVTEC for the station is positive during the storm. Results at Adis Ababa (AAE) show the maximum value of 56 TECU for VTEC on 23 June at 13:30 UT and a negative DVTEC value of -10.07 TECU on 22 September at 9.45 UT as shown in

Figures 4a and 4b are for the storm period from 20 – 23 September 2015. Figure 4a is similar to Figure 2a, and Figures 4b is similar to Figures 2b and with the respective stations KOUR and

AAE. The other two stations in the Asian longitude sector (CUSV and PBRI) faced data recording issues during this. In Figure 4a, the IMF Bz component is turning roughly south with a value near -20 nT during the early hours of 20 September. It fluctuates with less variation during the subsequent days until 23 September. Bz turns north and reaches the value of +15 nT around 15:00 UT. The SSC occurred on September 20th at 6:00 UT and is shown in Figures 4b and 4c with a vertical black line on the Dst index plot (top panels). The Dst index shows a minimum value of - 75 nT. It can be seen in Figure 4b in the 2nd panel, the behaviours of VTEC and the median are almost similar with a slight change periodically each day around 17.00 UT during the storm time. The VTEC reaches 60 TECU daily, while the median is a little less (about 50 TECU). The absolute maximum value for DVTEC was 21.95 TECU on 20 September at 17.45 UT. At AAE, the maximum VTEC value is 58.16 TECU on 23 September at 14.00 UT, and DVTEC has a negative response with a value of 8.5 TECU on 21 September at 13.00 UT as can be seen in the 3rd panel.

3.2 Generalisation for all the storms

Similar to the analysis done in section 3.1, we studied all the storms as listed in Table 2, to obtain a statistical representation of storm time variability in VTEC, DVTEC and corresponding time delays. For all the selected storms (see Table 2), we made a unique analysis for the three storms presented in Section 3.1. Section 3.2 brings together the statistical results for all the storms. Tables 3, 4, 5, and 6 give the values of specific parameters concerning the different storms at KOUR, CUSV, PBRI and AAE, respectively. The extreme right column in the tables indicates the event's status in correlation, either selected or excluded, following the criteria given below. in the rows with bold fonts indicate that the specific event is observed at several stations. Among the 36 magnetic storms, some events were excluded by using 2 criteria: a) SSC occurs on the dayside or nighttime from 22:00 LT to 05:00 LT and b) the origin of the magnetic storm on the solar disk must be far from the limb or do not belong to the far side. Only 29 events among 36 magnetic storms (Table 2) are selected for geomagnetic storm correlation enhancement. The other events are inconsistent as with special conditions that cannot be generalised and could be rather discussed in a collection with other events having similar characteristics. Selection of such criteria has significantly improved the correlation values, presented subsequently in this study.

Figures 5, 6, and 7 show the correlations between the Dst minimum and the response time of the ionosphere, which is the time between the time of the SSC and the absolute maximum

DVTEC.-Figure 5 shows the correlation between the KOUR station in South America for all the events (5a) and the selected events (5b). The correlation for all 15 events is 0.217, and the correlation for the 9 chosen events is 0.759. In Figure 6, we represent the correlation for all the events (6a) and the selected events (6 b) at CUSV, the corresponding value for all 11 events is 0.44, and that for the 9 chosen events is 0.842. Figure 7 shows that at PBRI, the correlation for all 6 events is 0.18 and that for the 5 selected events is 0.797. Figure 8 depicts that at AAE, the correlation value is 0.508 for all the events and 0.641 for the 6 selected events. Table 7 shows the stations, number of events, correlation for all events, and all events chosen with their new correlation. It clearly shows the importance of our chosen criteria to increase the correlation.

Figure 9a shows four plots on the ionospheric response, defined as the delay between the SSC and the absolute maximum of DVTEC in hours versus day of the year (DOY) during the period from 2014 - 2017. Figure 9b represents the onset time of the SSC in UT versus the day of the year (DOY) in four plots. The blue is for the selected events, and the red is for the excluded ones from 2014 - 2017. We have underlined by lines the tendencies concerning the selected cases. We see that these trends for the years 2015 and 2016 are identical in Figures 9a and 9b. We also note that in Figure 9a for the year 2017, almost all the selected events are aligned.

4. Discussion

We studied the ionospheric time delay response (Δt_{iono}) for 36 geomagnetic storms from 2014 - 2017, of which 29 events are selected based on the selection criteria presented in the previous section. The equatorial VTEC is derived from dual-frequency GPS stations at different longitude sectors along the magnetic equator, i.e., KOUR in the South American longitude sector, AAE in the African longitudes, and PBRI as well as CUSV in the Asian longitude sector. **Balan & RAO, (1990)** investigated TEC for 68 storms during the period between 1968-1972 at the low-latitude station of Hawaii, Honolulu (19.7 N, 157.2 W) and 62 storms at the mid-latitude station of Hamilton (38.7°N, 70.0°W). Their results realized that at low latitudes, 35 ionospheric storms are positive, and 33 are negative. However, during the same period, 32 ionospheric storms are positive and 30 are negative at middle latitudes. It was found that the response at low latitudes is generally positive for the SSCs that occur between midnight and midday and negative for those that occur at other times, whereas, at mid-latitudes, the response is usually positive for daytime SSCs and negative for nighttime SSCs. Their results demonstrate an ionospheric delay of about 35 hr after the SSCs. In comparison with our work, we found that the response time is ~ 27 hr less than Balan and Rao's of 8 hours. The list of magnetic storms

with their characteristics is mentioned previously in Part 2. **Fuller-Rowell et al., (1994)** studied the impact of magnetic storms on mid- and low-latitude ionospheric compositions at different SSCs times. They showed that the Travelling Atmospheric Disturbance (TAD) moves towards the nightside. This TAD takes about 3 hours to arrive at low latitudes where it causes changes in composition, and then this change rotates with the earth; therefore, the 27 hours could correspond to 3 hours plus 24 hours. We found ionospheric disturbances, either negative or positive, that do not show a significant difference in the response time for relative DVTEC values (shown in Tables 3, 4, 5, and 6). So, we summed up the response time for all the magnetic storms during the indicated period (2014 - 2017) to get the average. **Jimoh et al., (2016)** studied TEC at Ile-Ife/ Nigeria (Lat. 7.55° N, Long. 4.55° E, Dip. Lat. 7.50° N) for two major events on March 9th and October 1st, 2012. Their results show that IMF-Bz magnitude, duration, and orientation played an essential role in the dynamics and electrodynamics associated with these geomagnetic storms. In terms of the response of TEC during these storms, there were obvious positive departures from the mean quiet TEC. The maximum deviation percentage in TEC was about 120% and 45% on 9 March and 1October, 2012, respectively. A noticeable negative TEC rate deviation was observed after SSC arrival.

Our work showed the maximum deviation from the quiet time TEC with the DVTEC reaching a level of 120 % for the storm in March 2015 as shown in Figures 2b and 2c, which is in line with the reports of **Jimoh et al., (2016)**. However, we could not find a relation between the storm duration and the delay in ionospheric response time. Also, there was no clear correlation between the value of TEC and the delayed ionospheric response time. **Liu et al., (2010)** studied the time delay and duration of ionospheric density variations owing to the geomagnetically disturbed conditions from 28 August 1998 to 31 December 2008 using the global ionosphere maps periodically released by JPL-NASA. Their analysis infers that the duration of both the negative phase and positive phase has a clear latitudinal, seasonal, and magnetic local time (MLT) dependence. During the daytime and post-sunset hours at mid and low latitudes, the time delay is about 10 h for cases $20 \leq Ap < 40$ and nearly 12 h for cases $Ap \geq 40$. In the winter hemisphere, the negative phase propagation delay is between 1–10 h depending on the local time of latitude and storm intensity as like in the summer hemisphere. From the morning to midnight sector at middle to low latitudes, the negative phase shows a longer delay, reaching 9–12 h and 13–15 h for situations $20 \leq Ap < 40$ and $Ap \geq 40$, respectively. At the auroral latitudes in the night sector, the time delay for the negative phase is postponed to around 12 h for situation $20 \leq Ap < 40$ and about 16h for $Ap \geq 40$. The duration of the positive/negative ionospheric

disturbance is not of interest in this work; however, we did not find a relation between the value of the DVTEC and the local time of the SSC occurrence. Classifying the magnetic storms according to the seasons showed that negative ionospheric disturbances occur mainly in spring and winter which is still not included in the focal point of research in this study. The magnetic storms in this study were caused by 29 CMEs, 6 coronal holes (CH), and High-Speed Solar Wind (HSSW). Due to an error in the data on 15 February 2014, the actual number of events considered is 35 instead of 36. The CMEs mainly occurred, causing the Dst minimum in the range of -25 to -222 nT and the HSSW Dst minimum in the -30 to -100 nT field. Most of the magnetic storms are caused by CME and the day sided at KOUR station (16 events) and CUSV in Thailand (6 events). Note that in this research, we hadn't followed the magnetic storm classification criteria for Gonzalez et al. (1994), rather a threshold value of Dst (-20 nT) was sufficient to select the intended events in this work.

The present work takes into consideration solar and magnetic indices and statistically evaluates the response time (Δt_{iono}) of the variation of DVTEC along the equatorial location at three longitude sectors. We established a correlation and equation based on the delays Δt_{iono} measured at each station during different geomagnetic storms. The extreme value of TEC is 38.5 TECU for the magnetic storm on 27 February 2014 when the Dst minimum is -99 nT even though it is excluded as it was an east-limbed CME. We agree that the delay in the ionosphere due to the [O/N2] depletion region remains fixed in the geographic coordinate. The depletion corotates with the earth at a speed slightly slower than the earth's rotational speed **(Zhang, 2004)**. The selection criteria showed an enhancement in the correlation results. Parts (a) for Figures 5 to 8 show the correlation for all the events with their expected equations, and the selected events correlation showed in parts (b) from Figures 5 to 8.

The highest correlation value is in the Thailand region (R=0.84), followed by the Indian region (R=0.79), and the South American region (R=0.759), with the lowest value for the African region (0.641). We found that most negative storms lie in the 8 - 16 LT time range in all the longitude sectors. This study shows a significant correlation between the Dst and the response time and the equations deduced to describe the ionosphere in these regions. Neither the correlation nor the equation was introduced before. The response time for geomagnetic storms is related to the mechanism of the energetic particles that have access through the system, where the value of the particle intensity is expressed in terms of Dst index, as the magnetosphere-ionosphere system becomes conductive. When a storm has an interval of time due to a

sufficiently intense and long-lasting interplanetary convection electric field through a substantial energization in the magnetosphere-ionosphere system, the energy in the system intensifies the ring current strong enough to exceed some key threshold (- 20 nT in this paper) of the quantifying storm time Dst index.

The DVTEC and Dst show some relation, where the amplitude of Dst index approximately corresponds to a certain magnitude of DVTEC, which detects scopes for more research establishment in the near future. It is noteworthy to mention that the selection criterion for the storm's contribution in this research is carefully defined with the SSC occurring on the day side, as well as that the origin of the magnetic storm on the solar disk being far away from the limb or does not belong to the far side. We selected the DVTEC following the criteria that the DVTEC must not be less than 20% of the observed VTEC value (8 TECU).

5. Conclusion

The present paper investigates the ionospheric response time to the onset of geomagnetic storms of diverse levels of intensity during the period from 2014 to 2017 by considering the GPS derived TEC observations at four equatorial stations corresponding to three longitude sectors. We presented the most intense storms during the reviewed period, a correlation between the ionospheric response time and Dst is deduced at each equatorial station, from which a suitable mathematical equation has been derived to represent the strength of association ship between the two parameters. The correlation values seem to be strong by using the selected criteria in this study.

The important findings in the present paper can be summarized as follows:

i. The response time (time between the SSC and the absolute maximum DVTEC) for all the magnetic storms during the indicated period (2014 - 2017) is 27.2 hr.

ii. The ionospheric disturbance, either negative or positive, does not show a significant difference in the response time for a comparable DVTEC value.

iii. The limb and far-sided solar events that caused magnetic storms and nighttime SSC have different behaviour for the response time versus Dst relation.

iv. The correlation between the Dst minimum and the response time of the ionosphere becomes significant by defining an appropriate criterion, with the SSC on the dayside and the location of the solar source on the sun (see Table 7).

v. The response time does not show a repetitive behaviour or relation during the period 2014 - 2017 with the DOY (Fig 9a) as well as the SSC onset time in UT and DOY (Fig 9b)

Acknowledgement

Our research has become easier by referring to all the websites with free available data. My research would have been impossible without the aid and support of the following links:
The authors thank ISGI (International Service on rapid magnetic variations) for adding the archive of SSC list for all magnetic storms at http://isgi.unistra.fr/isgi_refservice.php. The authors thank Celestrak for GPS Yuma almanac archived https://celestrak.com/GPS/almanac/Yuma/. The authors thank http://ftp.aiub.unibe.ch for providing the codg and DCB files for providing the GPS. Also, we thank IGS for providing data online at https://cddis.nasa.gov/. Authors thank solarham.com for providing a report on solar activity and interplanetary medium archive http://www.solarham.net. C. Amory-Mazaudier thanks the ISSI-Bern International Team of "Why Ionospheric Dynamics and Structure Behave Differently in The African Sector?" (the team leaders E. Yizengaw & K. Groves) for valuable discussion on the part of the results included in this paper. I am profoundly grateful to Ms Heba Shalaby for helping with the Matlab codes.

References

Aa, E., Zhang, S.-R., Shen, H., Liu, S., & Li, J. (2021). Local and conjugate ionospheric total electron content variation during the 21 June 2020 solar eclipse. *Advances in Space Research*, *68*(8), 3435–3454. https://doi.org/10.1016/j.asr.2021.06.015

Appleton, E. V., & Naismith, R. (1935). Some further measurements of upper atmospheric ionization. *Proceedings of the Royal Society of London. Series A - Mathematical and Physical Sciences*, *150*(871), 685–708. https://doi.org/10.1098/rspa.1935.0129

Balan, N., & RAO, P. B. (1990). *Dependence of ionospheric response on the local time of sudden commencement and the intensity of geomagnetic storms*. https://doi.org/10.1016/0021-9169(90)90094-4

Cander, L. R. (2016). Re-visit of ionosphere storm morphology with TEC data in the current solar cycle. *Journal of Atmospheric and Solar-Terrestrial Physics*, *138–139*, 187–205. https://doi.org/10.1016/j.jastp.2016.01.008

Chakraborty, M., Kumar, S., De, B. K., & Guha, A. (2015). Effects of geomagnetic storm on low latitude ionospheric total electron content: A case study from Indian sector. *Journal of Earth System Science*, *124*(5), 1115–1126. https://doi.org/10.1007/s12040-015-0588-3

Davis, C. J., Wild, M. N., Lockwood, M., & Tulunay, Y. K. (1997). Ionospheric and geomagnetic responses to changes in IMF BZ: a superposed epoch study. *Annales Geophysicae*, *15*(2), 217–230. https://doi.org/10.1007/s00585-997-0217-9

de Siqueira Negreti, P. M., de Paula, E. R., & Candido, C. M. N. (2017). Total electron content responses to HILDCAAs and geomagnetic storms over South America. *Annales Geophysicae*, *35*(6), 1309–1326. https://doi.org/10.5194/angeo-35-1309-2017

Duncan, R. A. (1969). F-region seasonal and magnetic storm behaviour. *Journal of Atmospheric and Solar-Terrestrial Physics*, *31*, 59–70. https://doi.org/10.1016/0021-9169(69)90081-6

Evans, J. V. (1965). Midlatitude ionospheric temperatures on magnetically quiet and disturbed days. *Journal of Geophysical Research*, *70*(11), 2726–2732. https://doi.org/10.1029/JZ070i011p02726

Fuller-Rowell, T. J., Codrescu, M. V., Moffett, R. J., & Quegan, S. (1994). Response of the thermosphere and ionosphere to geomagnetic storms. *Journal of Geophysical Research*, *99*(A3), 3893. https://doi.org/10.1029/93JA02015

Gonzalez, w. D., Joselyn, J. A., Kamide, Y., Kroehl, H. W., Rostoker, G., Tsurutani, B. T., & Vasyliunas, V. M. (1994). What is a geomagneticstorm. *Journal of Geophysical Research*, *99*, 5771–5792. https://doi.org/10.1029/93ja02867

Iyer, S., & Mahajan, A. (2021). Granger causality analysis of deviation in total electron content during geomagnetic storms in the equatorial region. *Journal of Engineering and Applied Science*, *68*(1), 4. https://doi.org/10.1186/s44147-021-00007-x

Jimoh, O. E., Yesufu, T. K., & Ariyibi, E. A. (2016). Investigation of Ionospheric Response to Geomagnetic Storms over a Low Latitude Station, Ile-Ife, Nigeria. *Acta Geophysica*, *64*(3), 772–795. https://doi.org/10.1515/acgeo-2016-0013

Kashcheyev, A., Migoya-Orué, Y., Amory-Mazaudier, C., Fleury, R., Nava, B., Alazo-Cuartas, K., & Radicella, S. M. (2018). Multivariable Comprehensive Analysis of Two Great Geomagnetic Storms of 2015. *Journal of Geophysical Research: Space Physics*, *123*(6), 5000–5018. https://doi.org/10.1029/2017JA024900

Koga, D., Sobral, J. H. A., Gonzalez, W. D., Arruda, D. C. S., Abdu, M. A., de Castilho, V. M., Mascarenhas, M., Gonzalez, A. C., Tsurutani, B. T., Denardini, C. M., & Zamlutti, C. J. (2011). Electrodynamic coupling processes between the magnetosphere and the equatorial ionosphere during a 5-day HILDCAA event. *Journal of Atmospheric and Solar-Terrestrial Physics*, *73*(1), 148–155. https://doi.org/10.1016/j.jastp.2010.09.002

Liu, J., Liu, L., Nakamura, T., Zhao, B., Ning, B., & Yoshikawa, A. (2014). A case study of Ionospheric storm effects during long-lasting southward IMF Bz driven geomagnetic storm. *Journal of Geophysical Research: Space Physics*, *119*(9), 7716–7731. https://doi.org/10.1002/2014JA020273

Liu, J., Zhao, B., & Liu, L. (2010). Time delay and duration of ionospheric total electron content responses to geomagnetic disturbances. *Annales Geophysicae*, *28*(3), 795–805. https://doi.org/10.5194/angeo-28-795-2010

Nava, B., Rodríguez-Zuluaga, J., Alazo-Cuartas, K., Kashcheyev, A., Migoya-Orué, Y., Radicella, S. M., Amory-Mazaudier, C., & Fleury, R. (2016). Middle- and low-latitude ionosphere response to 2015 St. Patrick's Day geomagnetic storm. *Journal of Geophysical Research: Space Physics*, *121*(4), 3421–3438. https://doi.org/10.1002/2015JA022299

Obayashi, T., & Matuura, N. (1970). Theoretical Model of F-Region Storms. In *Solar-Terrestrial Physics/1970: Proceedings of the International Symposium on Solar-Terrestrial Physics held in Leningrad, U.S.S.R. 12–19 May 1970* (Vol. 29). https://doi.org/10.1007/978-94-009-3693-5_43

Odeyemi, O. O., Adeniyi, J., Oladipo, O., Olawepo, O., Adimula, I., & Oyeyemi, E. (2018). Morphology of GPS and DPS TEC over an equatorial station: Validation of IRI and NeQuick 2 models. *Annales Geophysicae*, *36*(5), 1457–1469. https://doi.org/10.5194/angeo-36-1457-2018

Prölss, G. W. (1976a). ON EXPLAINING THE NEGATIVE PHASE OF IONOSPHERIC STORMS. *Planetary and Space Science*, *24*. https://doi.org/10.1016/0032-0633(76)90140-9

Prölss, G. W. (1976b). *Storm-time coupling of ionosphere and neutral atmosphere: ESRO 4 results, The Geophysical Use of Satellite Beacon Observations*.

Prölss, G. W. (1980). Magnetic storm associated perturbations of the upper atmosphere: Recent results obtained by satellite-borne gas analyzers. *Reviews of Geophysics*, *18*(1), 183. https://doi.org/10.1029/RG018i001p00183

Silwal, A., Gautam, S. P., Poudel, P., Karki, M., Adhikari, B., Chapagain, N. P., Mishra, R. K., Ghimire, B. D., & Migoya-Orue, Y. (2021). Global Positioning System Observations of Ionospheric Total Electron Content Variations During the 15th January 2010 and 21st June 2020 Solar Eclipse. *Radio Science*, *56*(5). https://doi.org/10.1029/2020RS007215

Sobral, J. H. A., Abdu, M. A., Gonzalez, W. D., Gonzalez, A. C., Tsurutani, B. T., da Silva, R. R. L., Barbosa, I. G., Arruda, D. C. S., Denardini, C. M., Zamlutti, C. J., & Guarnieri, F. (2006). Equatorial ionospheric responses to high-intensity long-duration auroral electrojet activity (HILDCAA). *Journal of Geophysical Research*, *111*(A7), A07S02. https://doi.org/10.1029/2005JA011393

Tsurutani, B. T., Gonzalez, W. D., Guarnieri, F., Kamide, Y., Zhou, X., & Arballo, J. K. (2004). Are high-intensity long-duration continuous AE activity (HILDCAA) events substorm expansion events? *Journal of Atmospheric and Solar-Terrestrial Physics*, *66*(2), 167–176. https://doi.org/10.1016/j.jastp.2003.08.015

Wei, Y., Hong, M., Wan, W., Du, A., Lei, J., Zhao, B., Wang, W., Ren, Z., & Yue, X. (2008). Unusually long lasting multiple penetration of interplanetary electric field to equatorial ionosphere under oscillating IMF Bz. *Geophysical Research Letters*, *35*(2), L02102. https://doi.org/10.1029/2007GL032305

Zhang, Y. (2004). O/N2 changes during 1–4 October 2002 storms: IMAGE SI-13 and TIMED//GUVI observations. *Journal of Geophysical Research*, *109*(A10), A10308. https://doi.org/10.1029/2004JA010441

Zolesi, B., & Cander, L. R. (2014). *Ionospheric Prediction and Forecasting*. Springer Berlin Heidelberg. https://doi.org/10.1007/978-3-642-38430-1

Tables captions

Table 1: List of the stations used in the study during the declining phase for solar cycle 24,

Table 2: Date and characteristics of the 36 storms selected during the period from 2014 - 2017.

Table 3*:* List of the geomagnetic storms observed in French Guiana (KOUR Station).

Table 4: Similar to Table 3 for the station CUSV in Asia.

Table 5: Similar to Table 3 for the station PBRI in Asia.

Table 6: Similar to Table 3 for the station AAE in Africa.

Table 7: The station used in the study with their correlation values and number of events in the case of all events and selected events.

Figure Captions

Figure 1: GPS stations used in this study for analyzing the total electron content (TEC): KOUR in French Guiana, AAE in Ethiopia, CUSV in Thailand and PBRI in India.

Figure 2a: Solar and magnetic parameters during the period of 17 - 20 March 2015, From the top to the bottom: IMF Bz component in nT, solar wind speed (V_{sw}) in km/s, Kp index and AE index in nT.

Figure 2b: KOUR, AAE and CUSV stations for the period 17 -20 March 2015, the top panel shows the Dst index, the 2^{nd} ,3^{rd} and 4^{th} panels show VTEC in blue color superimposed to median dashed line in red color and DVTEC in black color. The vertical black line represents the time of the SSC, the black dots are the maximum value for DVTEC for each station.

Figure 3a: Similar to Figure 2a for the storm from 22-25 June 2015

Figure 3b: KOUR, AAE and PBRI stations for the period 22-25 June 2015, top panel: Dst index, 2^{nd},3^{rd} and 4^{th} panels: VTEC in blue color is superimposed to the VTEC median in red color, and DVTEC in black color; The first vertical black line represents the time of the SSC, the second black dots are underlines the absolute value for DVTEC.

Figure 4a: Similar to Figure 2a for the storm from 20 -23 September 2015

Figure 4b: Similar to Figure 2b, KOUR and AAE stations for the period 20-23 September 2015, the black dot is the maximum of DVTEC.

Figure 5a: Dst versus response time (hr) in the South American sector for all 18 events from 2014-2017

Figure 5b: Dst versus response time (hr) for the 9 selected events in the South American sector

Figure 6a: Dst versus response time (hr) in the Asian Sector (CUSV) for all the 11 events from 2014-2017

Figure 6b: Dst versus response time in (hr,) for the 9 selected events in the Asian Sector (CUSV)

Figure 7a: Dst versus response time (hr) for all the 6 events in PBRI from 2014-2017

Figure 7b: Dst versus response time (hr) for the 5 selected events in PBRI from 2014-2017.

Figure 8a: Dst versus response time (hr) for all the 7 events in AAE from 2014-2017

Figure 8b: Dst versus response time (hr) for the 6 selected events in AAE from 2014-2017.

Figure 9: a) Illustrates the ionospheric response (time from SSC to the absolute maximum of DVTEC) in hours versus day of the year (DOY), for the period from 2014 - 2017, the blue is for the selected events and the red for the excluded ones.

Figure 9b) The onset time of SSC in UT versus the day of the year (DOY), the blue is for the selected events and the red for the excluded ones, for the period from 2014 - 2017.

Table 1

Station name	Country	Geographic coordinates		Geomagnetic coordinates		Mean Sea level Height (m)
		Latitude	Longitude	Latitude	Longitude	
AAE	Ethiopia	9.03°N	38.76°E	5.35°N	112.57°E	2439.15
CUSV	Thailand	13.73°N	100.53°E	4.48°N	173.75°E	76.06
PBRI	India	11.63°N	92.71°E	2.62°N	165.07°E	-22.55
KOUR	French Guiana	5.25°N	52.80°W	14.44°N	21.09°E	-25.57

Table 2

S.No.	SSC Date	SSC time in hh:mm	Dst index in nT	K_P index	Solar sources of Geomagnetic storm
1	15/2/2014	13:17	Data error	Data error	CME+M3.7 flare on 12/2/2014
2	20/2/2014	3:20	-91	6	Full halo CME on 18/2/2014
3	23/2/2014	7:05	-51	4+	CME +M3 flare on 20/2/2014
4	27/2/2014	16:50	-94	5+	Halo CME+X4.9 flare at 1967 sunspot on 25/2/2014
5	20/4/2014	10:56	-25	5	Halo CME+M7.3 flare on 18/4/2014
6	7/6/2014	16:52	-38	6+	CME on 4/6/ 2014
7	12/9/2014	15:53	-57	6+	CME+m4.5 flare on 9/9/2014
8	10/11/2014	2:21	-57	4+	CME+X1.6 flare due to region 2205 on 7/11/2014
9	21/12/2014	19:11	-29	4-	Faint Halo CME+M1.3 flare due to region 2242 on 19/12/2014
10	7/1/2015	6:14	-99	6+	Pair of Coronal Hole+ M flare and C flare on 5/1/2015
11	17/3/2015	4:45	-222	8-	CME +X2.2 flare on 13/3/2015
12	6/5/2015	1:42	-28	5+	CME+ Minor C flare Due to 2335 region on 3/5/2015
13	22/6/2015	18:33	-204	8	CME+ M 3.0 flare due to region 2371 on 21/6/2015
14	20/9/2015	6:03	-75	7	CME + C flare on 18/9/2014
15	3/11/2015	1:34	-60	5	CME + M flare due to region 2443 on 1/11/2015
16	6/11/2015	18:18	-89	4+	CME+M1.9 flare around region 2445 on 4/11/2015
17	14/12/2015	13:21	-47	5+	CME+C7.8 flare on 12/12/2015
18	19/12/2015	16:16	-155	6	CME+C6.6 flare and Full Halo CME on 16/12/2015
19	31/12/2015	0:50	-117	6-	Partial Halo CME +M1.8 flare on 28/12/2015
20	18/1/2016	21:57	-104	5-	Faint CME on 14 /1/2016
21	14/3/2016	17:14	-55	5	Minor C flare on 10/3/2016
22	14/4/2016	7:35	-52	5-	CME+C flare on 10/4/2016

23	19/7/2016	23:15	-26	5	CME+C6 flare on 17/7/2016
24	12/10/2016	22:12	-105	6+	Faint CME on 9/10/2016
25	9/11/2016	6:43	-57	5-	CME on 5/11/2016
26	26/1/2017	8:15	-33	4+	Coronal Hole 56 and minor C flare on 24/1/2017
27	27/5/2017	15:34	-122	7+	CME on 23/5/2017
28	9/7/2017	0:10	-31	5+	High speed solar wind from a Coronal Hole +B and occasional C flare on 7/7/2017
29	16/7/2017	0:59	-69	6	CME+M2.4 flare on 14/7/2017
30	31/8/2017	5:38	-60	5+	High speed solar wind from a Coronal Hole +C flare on 30/8/2017
31	7/9/2017	23:00	-142	8+	CME+X9.4 flare on 6/9/2017
32	12/9/2017	20:04	-50	5+	CME+X8.2 flare on 10/9/2017
33	14/9/2017	11:16	-53	6+	CME+C3 flare around 2680 sunspot on 12/9/2017
34	26/9/2017	23:48	-100	7-	High speed solar wind from a Coronal Hole 32 on 25/9/2017
35	21/10/2017	6:10	-18	3	CME on 18/10/2017
36	4/12/2017	16:13	-37	5-	High speed solar wind from a Coronal Hole 45 on 2/12/2017

Table 3

S. No.	Storm date	SSC time in UT and LT at the station	Extreme DVTEC value in TECU	Time of DVTEC Occurrence	Delay in hr	KOUR Station selection
1	15/2/2014	13:17UT 10:17 LT	Data error	Data error	Data error	excluded
2	27/2/2014	16:50 UT 13:50 LT	38.5	28/2/2014 00:45	8	excluded
3	20/4/2014	10:56 UT 7:56 LT	-20.88	21/4/2014 16:00	29	excluded
4	7/6/2014	16:52 UT 13:52LT	20.8	9/6/14 18:45	50.25	selected
5	12/9/2014	15:53 UT 12:53LT	12.8	12/9/14 19:00	3.16	excluded
6	21/12/2014	19:11UT 16:11 LT	25.6	24/12/2014 00:00	52.81	selected
7	17/3/2015	4:45 1:45 LT	23.94	18/3/2015 00:30	21.25	**excluded (KOUR, AAE & CUSV)**
8	22/6/2015	18:33 15:33LT	-29.14	23/6/2015 18:45	24.15	**Selected (AAE, KOUR &PBRI)**
9	20/9/2015	6:03 03:03 LT	21.95	20/9/2015 17:45	11.75	excluded
10	6/11/2015	18:18UT 15:18 LT	20.68	8/11/15 1:15	30.95	selected
11	14/12/2015	13:21UT 10:21 LT	20.1	15/12/2015 1:45	12.4	excluded
12	19/12/2015	16:16UT 13:16 LT	28.6	21/12/2015 00:00	31.48	selected
13	18/1/2016	21:57UT 18:57LT	16.47	20/1/2016 23:45	49.75	selected
14	14/3/2016	17:14UT 15:14 LT	-22.64	17/3/2016	72.5	selected
15	27/5/2017	15:34UT 12:34 LT	-9.26	28/5/2017 19:15	27.69	selected

16	7/9/2017	23:00UT 20:00 LT	19.23	8/9/2017 20:45	21.75	selected
17	12/9/2017	20:04UT 17:04LT	-13.91	16/9/2017 17:00	93	excluded
18	4/12/2017	16:13UT 13:13LT	6.6	5/12/17 1:45	9.54	excluded

Table 4

S. No.	Storm date	SSC time in UT and LT at the station	Extreme DVTEC value in TECU	Time of DVTEC occurrence	Delay of the response (hr)	CUSV Station selected
1	23/2/2014	7:05UT 14:34 LT	30.83	24/2/2014 1:30	18.41	selected
2	17/3/2015	4:45UT 12:15 LT	-29.11	18/3/2015 14:30	33.75	**Selected** **(KOUR, AAE & CUSV)**
3	31/12/2015	0:50UT 8:20 LT	-13.75	1/1/16 3:30	26.6	selected
4	14/4/2016	7:35UT 15:05 LT	13.25	14/4/2016 11:45	4.16	excluded
5	19/7/2016	23:45UT 7:15LT NEXT DAY	17.96	20/7/2016 11:00	11.75	selected
6	12/10/2016	22:12UT 5:40 LT NEXT DAY	19.65	14/10/2016 1:45	27.55	selected
7	9/7/2017	0:10UT 7:40 LT	5.6	9/7/17 13:15	13.08	selected
8	16/7/2017	00:59UT 8:29 LT	9.39	16/7/2017 11:45	10.75	selected
9	31/8/2017	5:38UT 13:08 LT	14.5	2/9/17 11:45	54.11	excluded
10	6/9/2017	23:44UT 7:14LT NEXT DAY	13.05	8/9/17 5:30	29.75	selected
11	26/9/2017	23:48 UT 7:18 LT NEXT DAY	14.5	28/9/2017 7:30	31.7	selected

Table 5

S.No.	Storm date	SSC time in UT and LT at the station	Extreme DVTEC value in TECU	Time of DVTEC occurrence	Response Delay in hr	PBRI selected station
1	20/2/2014	3:20UT 8:30LT	20.24	20/2/2014 14:00	11	selected
2	10/11/2014	2:21UT 7:50 LT	31.69	10/11/14 13:45	11.55	selected
3	7/1/2015	6:14UT 11:44 LT	12.75	7/1/15 6:45	0.5	selected
4	6/5/2015	1:42UT 7:12 LT	26.78	6/5/15 16:45	15.05	selected
5	22/6/2015	18:33 UT 23:33 LT	13.59	23/6/15 6:15	11.75	**excluded (AAE, KOUR & PBRI)**
6	3/11/2015	1:34UT 7:04 LT	23	3/11/15 12:30	10.9	selected

Table 6

S.No.	Storm date	SSC time in UT and LT at the station	Extreme DVTEC value in TECU	Time of DVTEC occurrence	Response delay in hr	AAE stations selected
1	17/3/2015	4:45UT 7:45 LT	29.52	17/3/2015 17:30	12.75	**Selected/ representative (KOUR, AAE & CUSV)**
2	22/6/2015	18:30UT 21:33 LT	-13.88	23/6/2015 07:00	13	**Selected (AAE, KOUR & PBRI)**
3	20/9/2015	6:03UT 9:03 LT	-10.07	22/9/2015 9:45	51.7	**Selected (KOUR & AAE)**
4	9/11/2016	6:43 UT 9:43 LT	9.61	11/11/16 8:45	50	selected
5	26/1/2017	8:15UT 11:15 LT	13.67	27/1/2017 16:15	32	selected
6	14/9/2017	11:16UT 14:16 LT	-9.97	15/9/2017 13:00	25.73	selected
7	21/10/2017	6:10UT 9:10 LT	8.02	22/10/2017 08:45	26.584	excluded

Table 7

Stations	Total Number of events and Correlation	Selected Number of events Correlation
KOUR	18 0.252	9 0.79
AAE	7 0.508	6 0.644
CUSV	11 -0.442	9 -0.845
PRIB	6 0.181	5 0.797

Figure 1

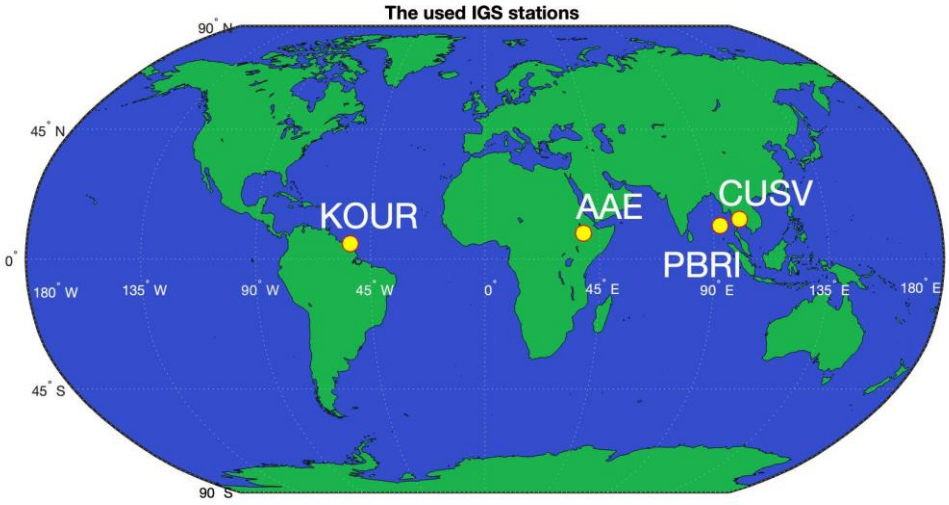
The used IGS stations
90° N
45° N
0°
45° S
90° S
180° W
135° W
90° W
45° W
0°
45° E
90° E
135° E
180° E
KOUR
AAE
CUSV
PBRI

Figure 2a

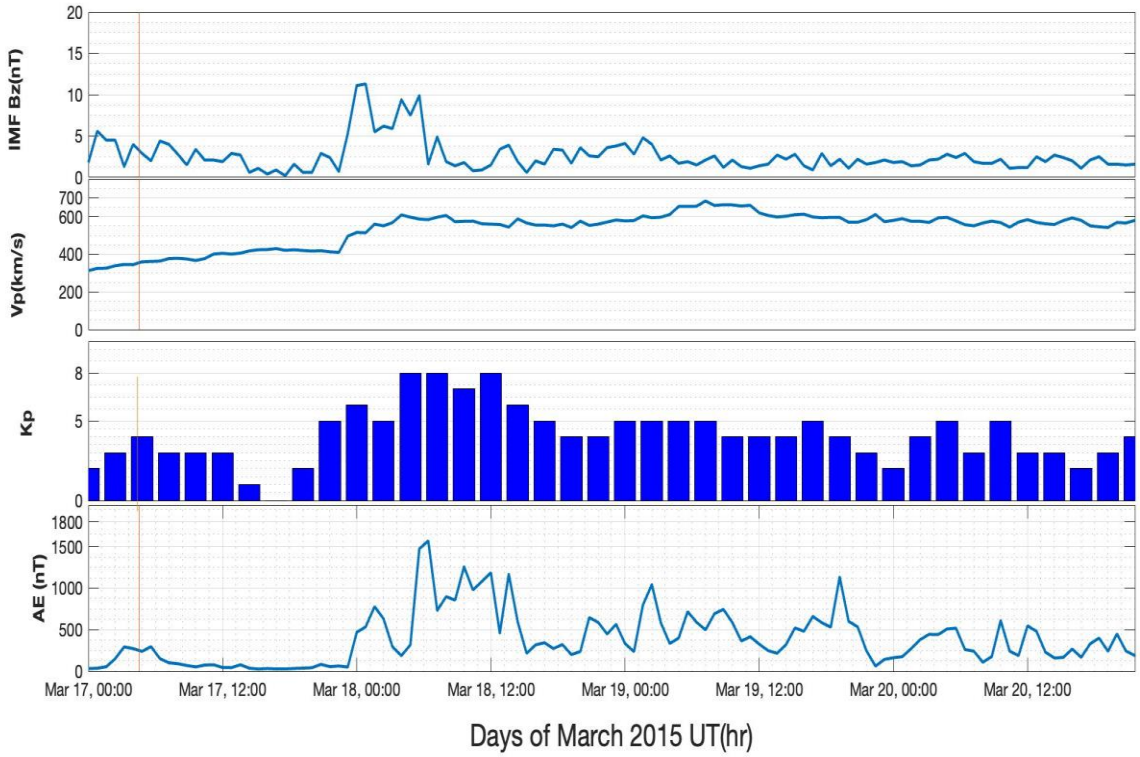

Figure 2b

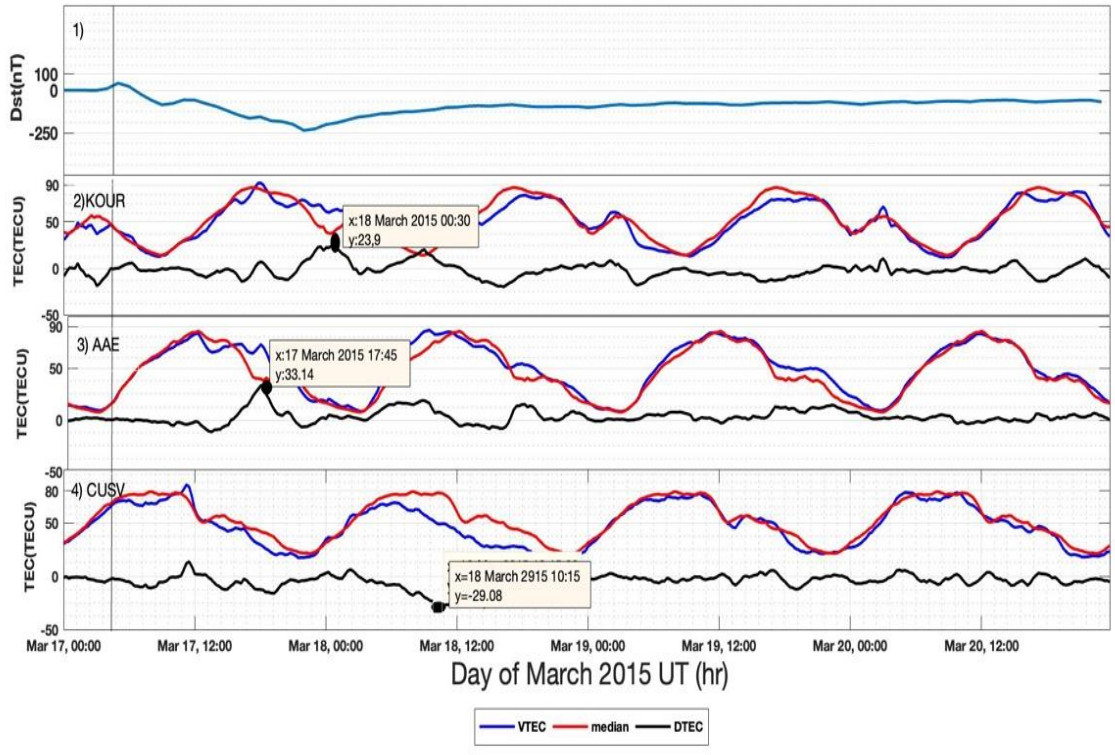

Figure 3a

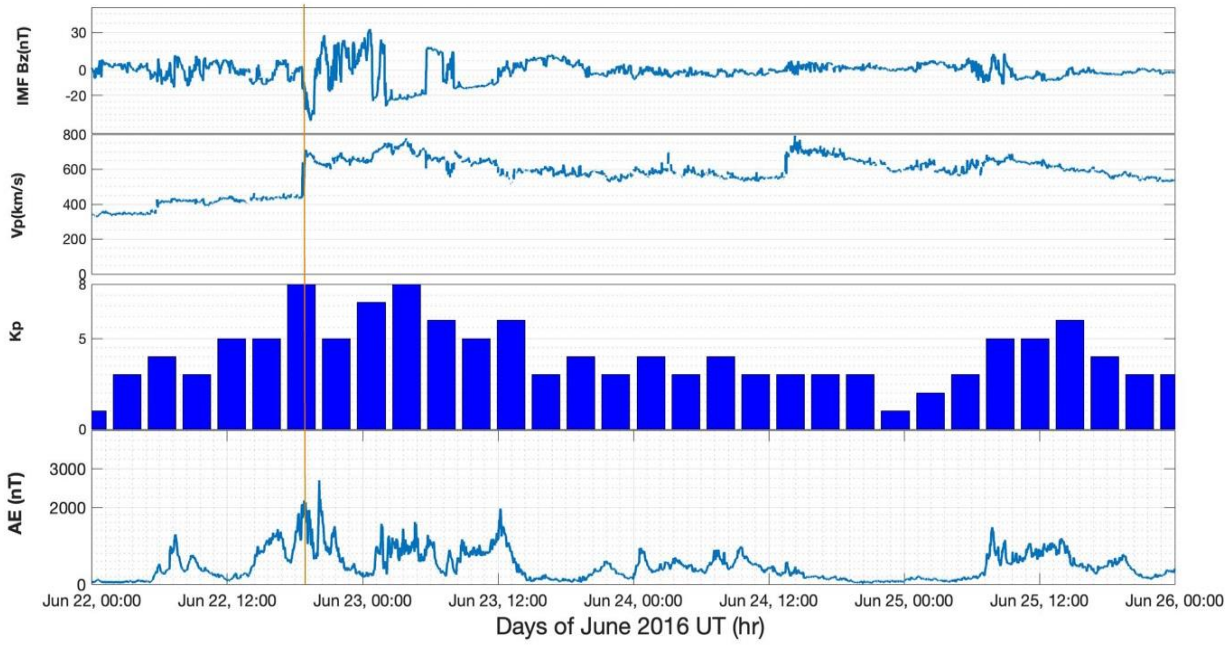

Figure 3b

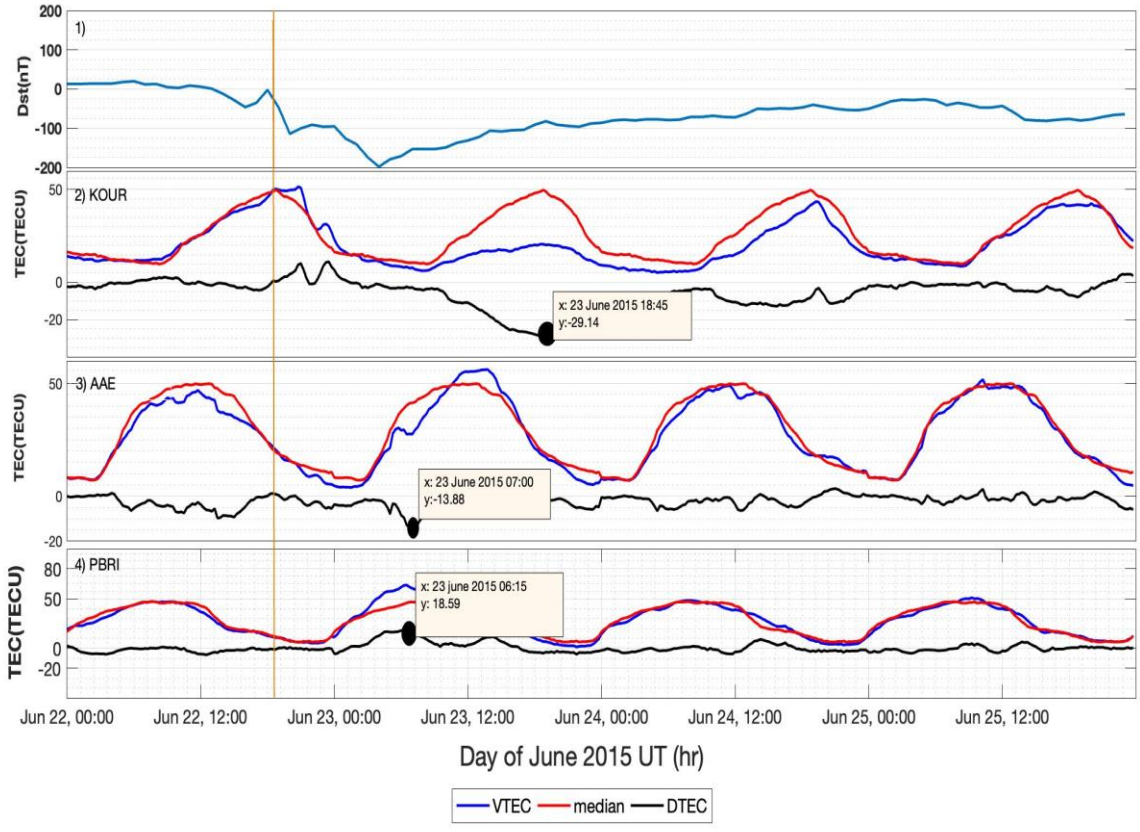

Figure 4a

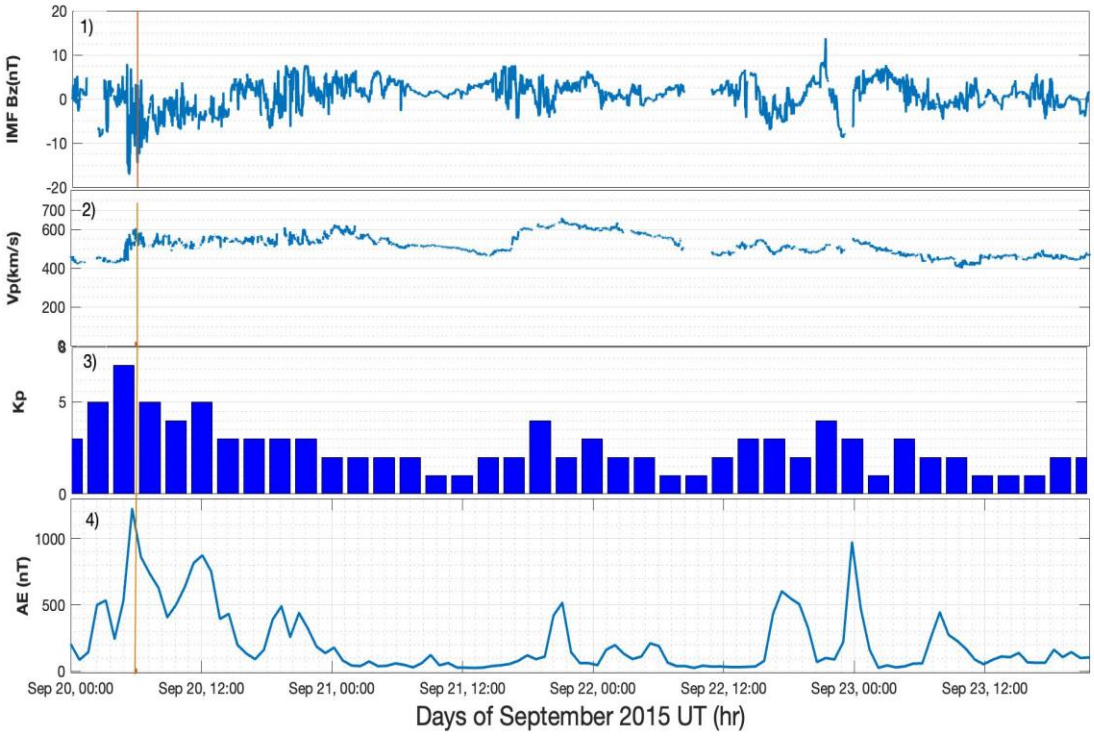

Figure 4b

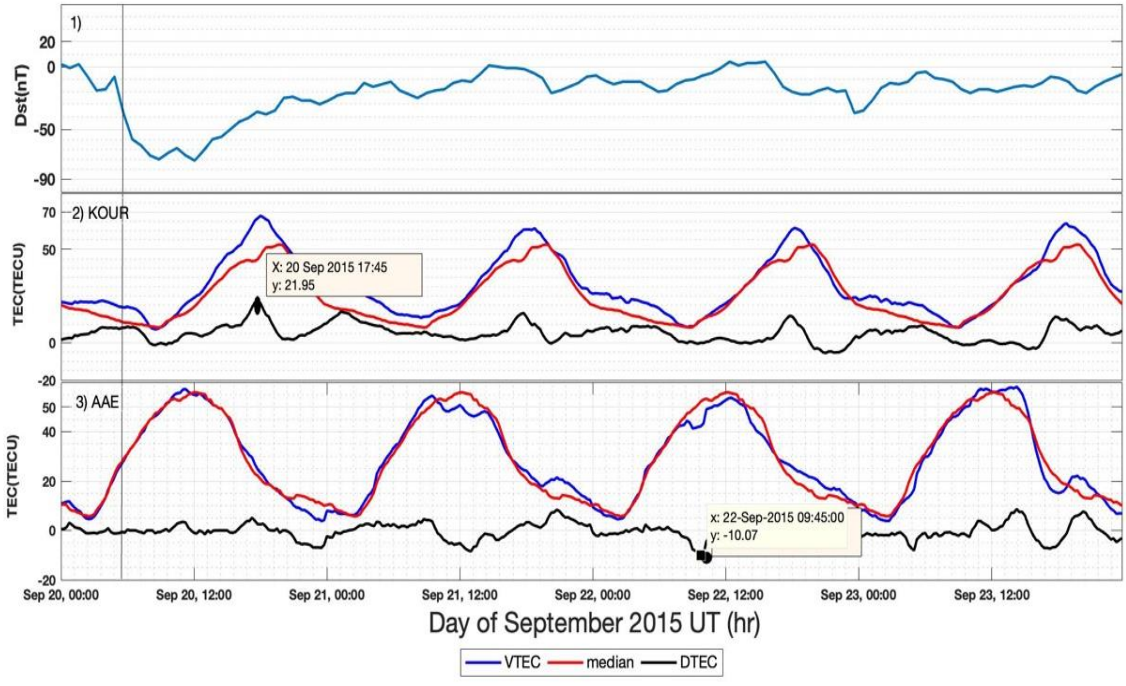

Figure 5a

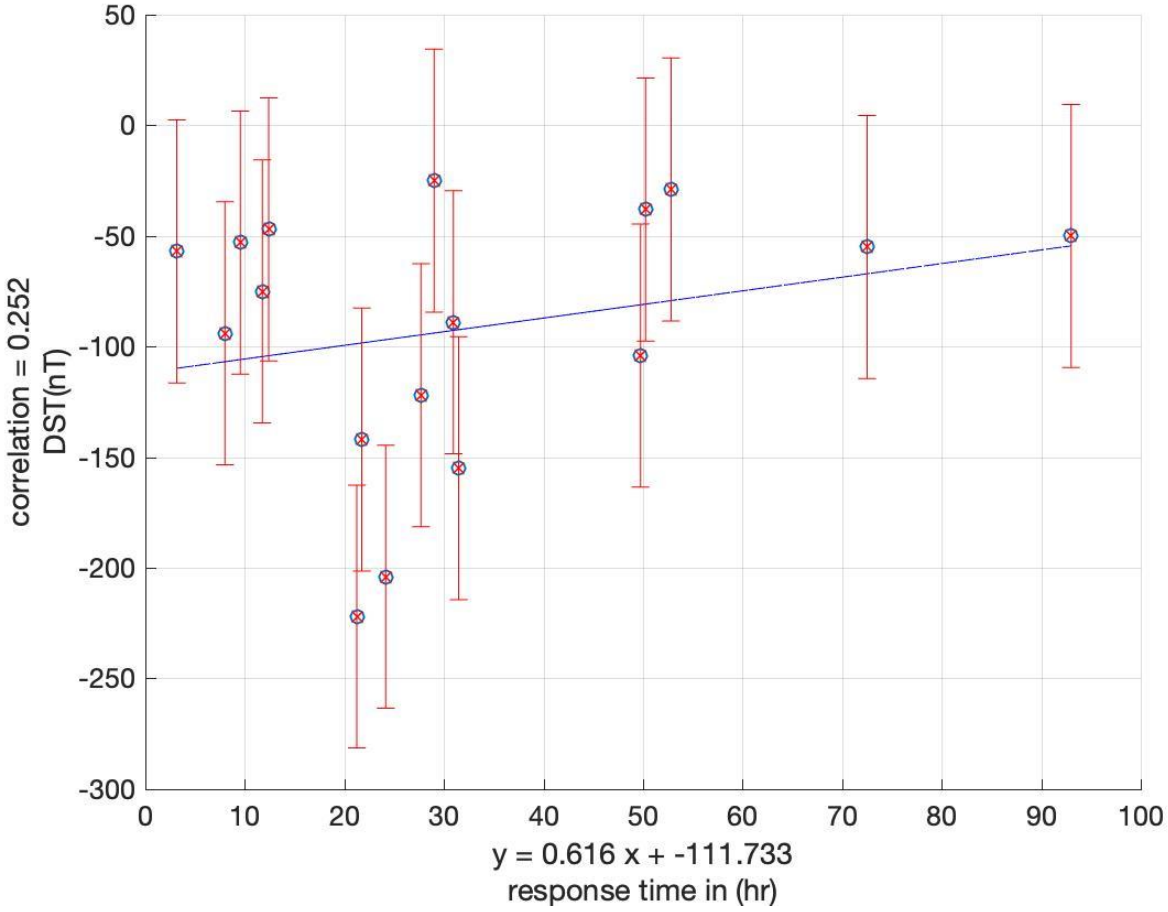
50
0
-50
-100
-150
-200
-250
-300
0
10
20
30
40
50
60
70
80
90
100
correlation = 0.252
DST(nT)
y = 0.616 x + -111.733
response time in (hr)

Figure 5b

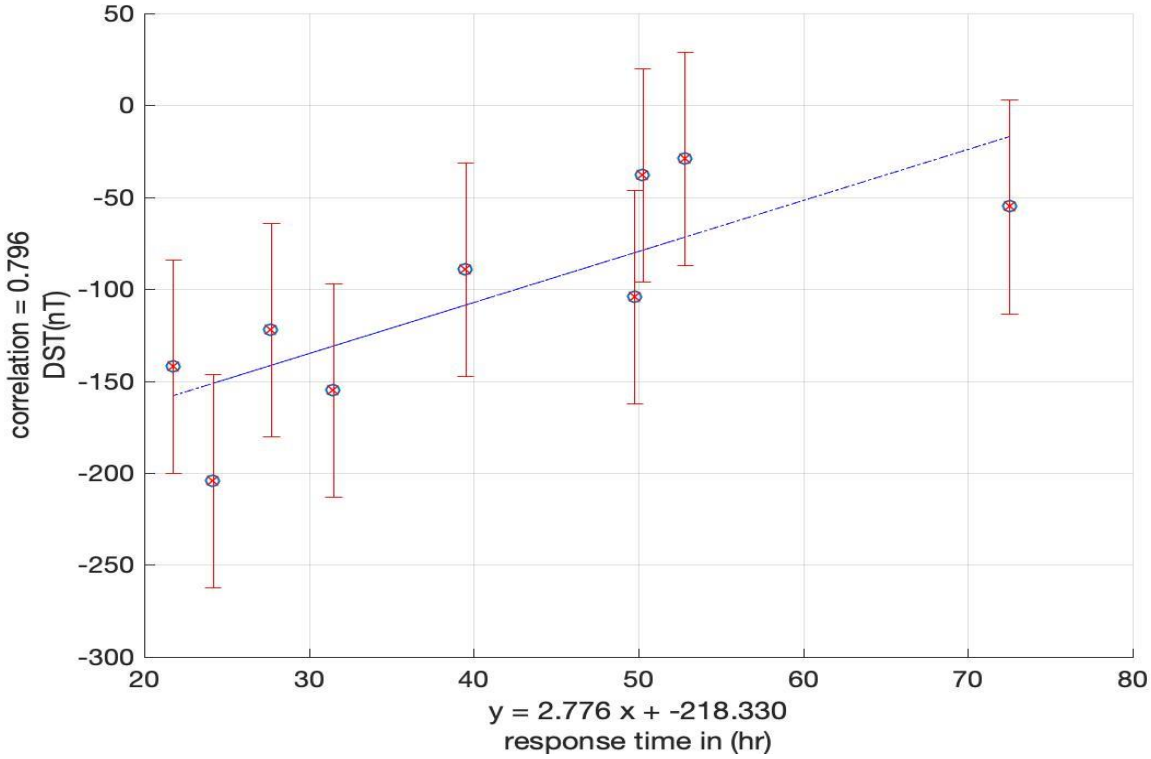
50
0
-50
-100
-150
-200
-250
-300
20
30
40
50
60
70
80
correlation = 0.796
DST(nT)
y = 2.776 x + -218.330
response time in (hr)

Figure 6a

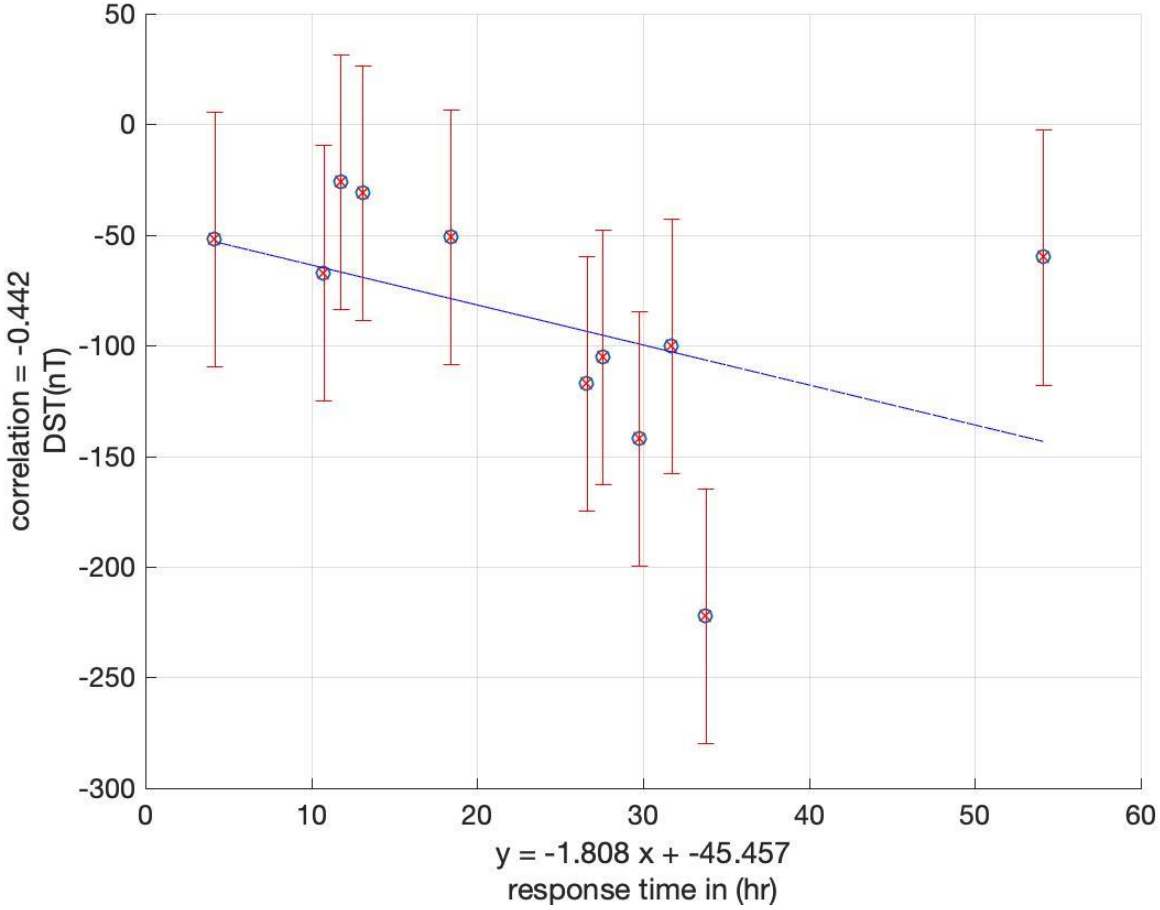
50
0
-50
-100
-150
-200
-250
-300
0
10
20
30
40
50
60
correlation = -0.442
DST(nT)
y = -1.808 x + -45.457
response time in (hr)

.

Figure 6b

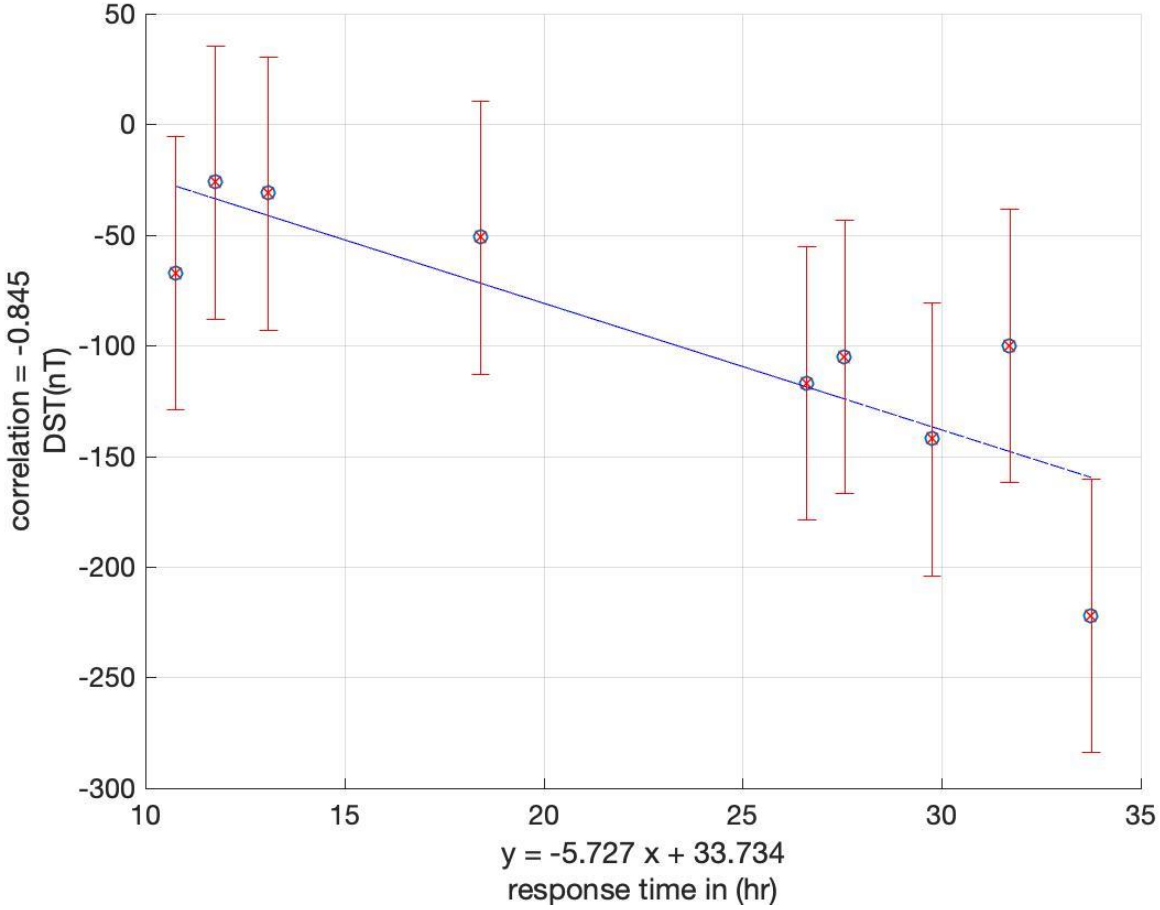
50
0
-50
-100
-150
-200
-250
-300
10
15
20
25
30
35
correlation = -0.845
DST(nT)
y = -5.727 x + 33.734
response time in (hr)

Figure 7a

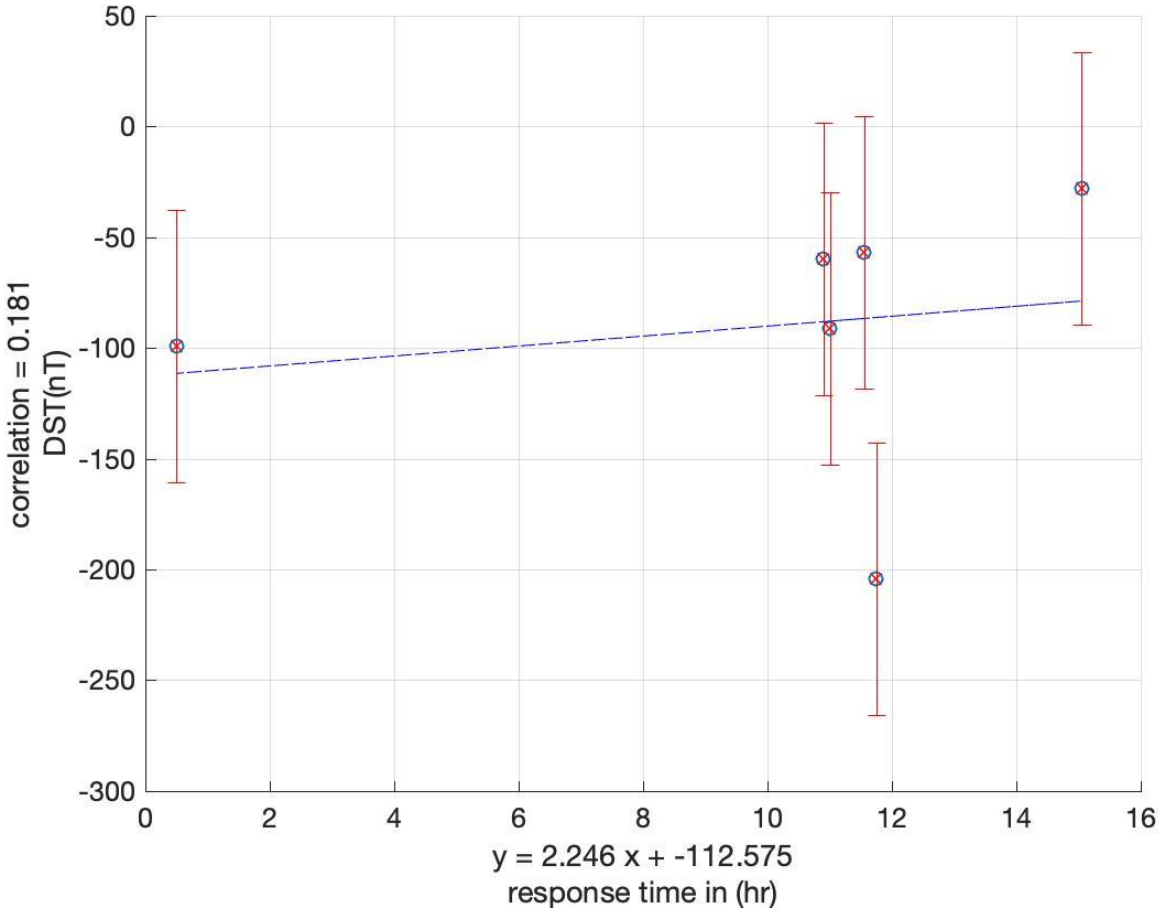
50
0
-50
-100
-150
-200
-250
-300
0
2
4
6
8
10
12
14
16
correlation = 0.181
DST(nT)
y = 2.246 x + -112.575
response time in (hr)

Figure 7b

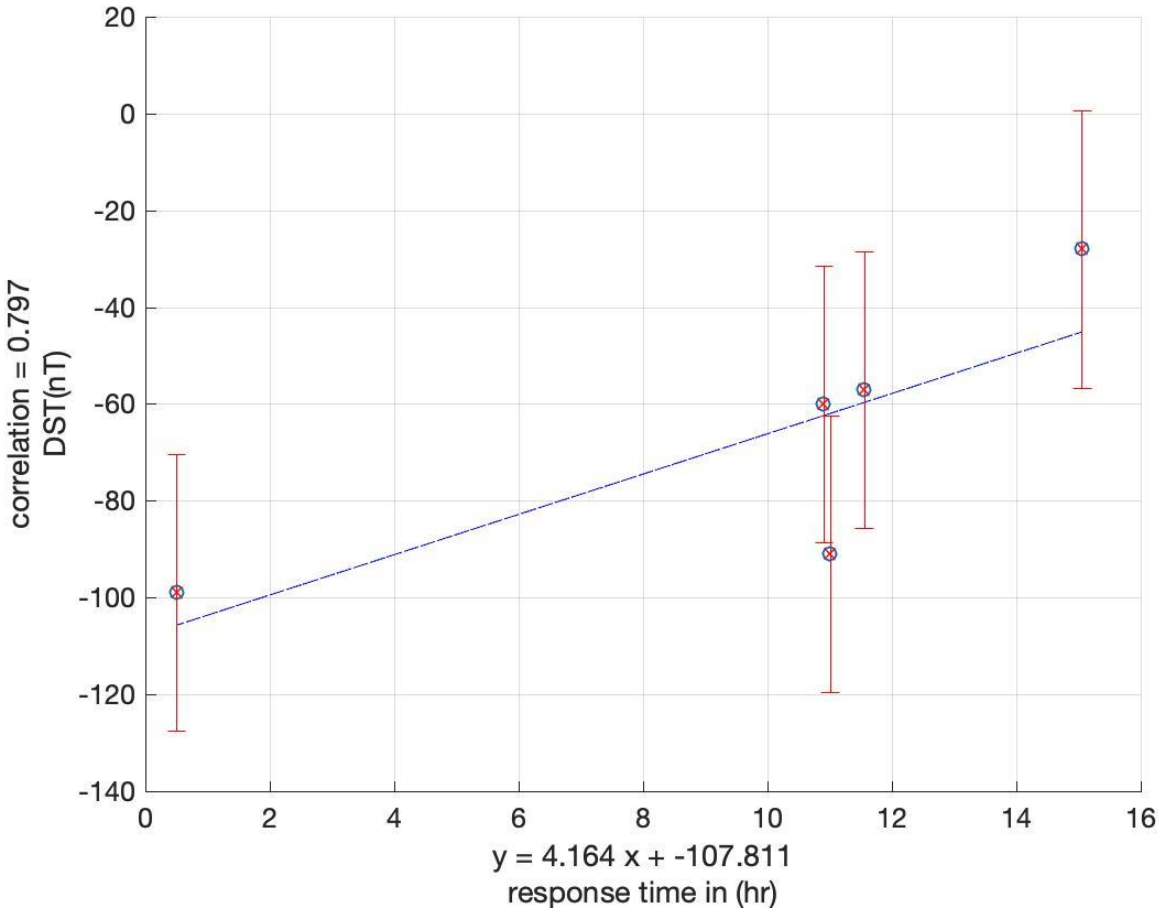
correlation = 0.797
DST(nT)
20
0
-20
-40
-60
-80
-100
-120
-140
0
2
4
6
8
10
12
14
16
y = 4.164 x + -107.811
response time in (hr)

Figure 8a

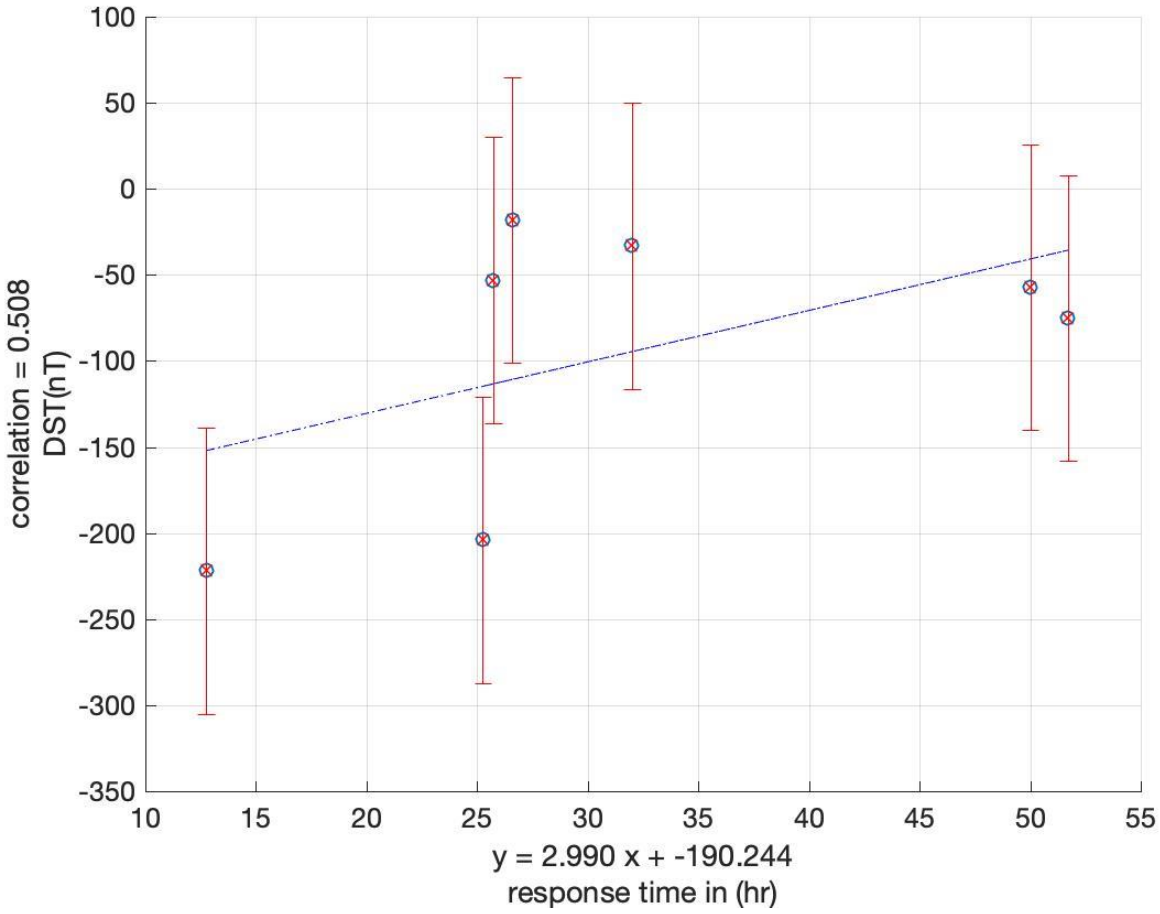
correlation = 0.508
DST(nT)
100
50
0
-50
-100
-150
-200
-250
-300
-350
10
15
20
25
30
35
40
45
50
55
y = 2.990 x + -190.244
response time in (hr)

Figure 8b

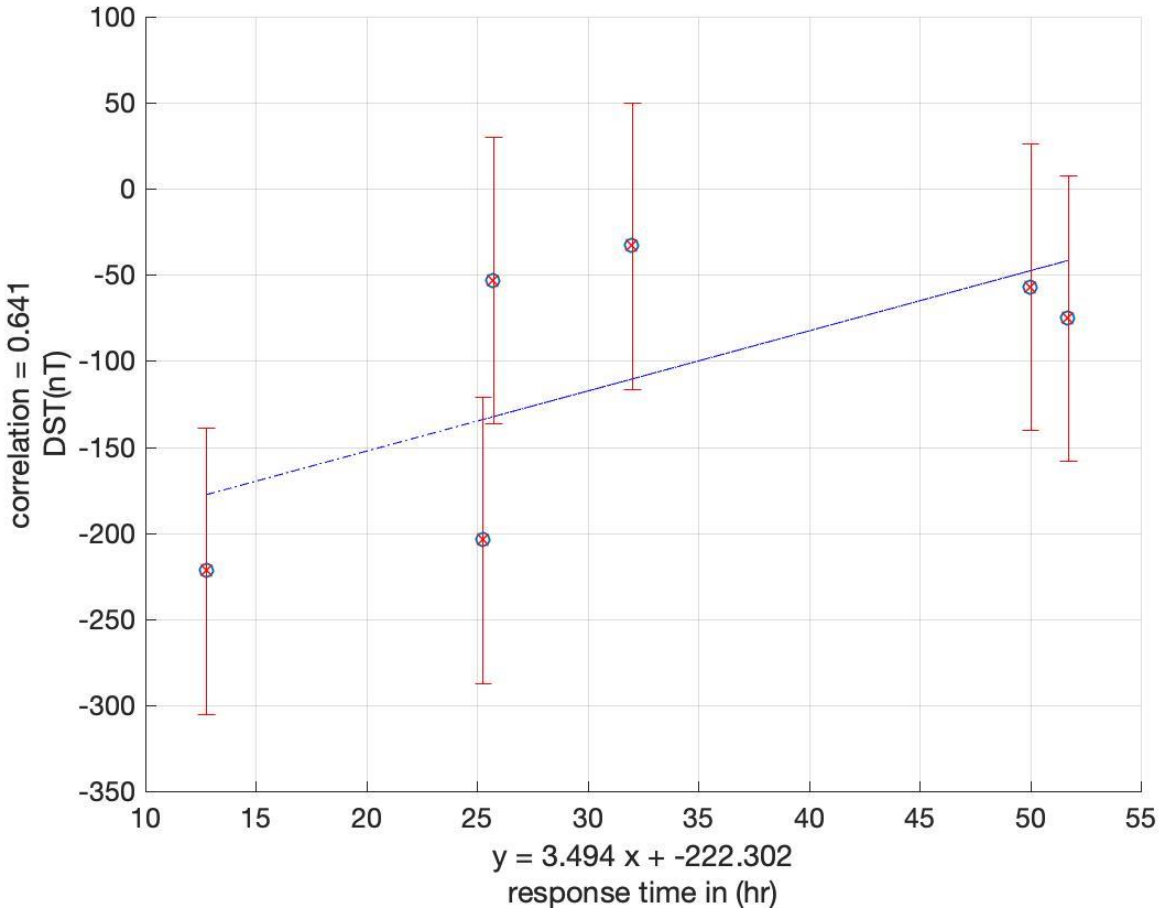
correlation = 0.641
DST(nT)
100
50
0
-50
-100
-150
-200
-250
-300
-350
10
15
20
25
30
35
40
45
50
55
y = 3.494 x + -222.302
response time in (hr)

Figure 9a

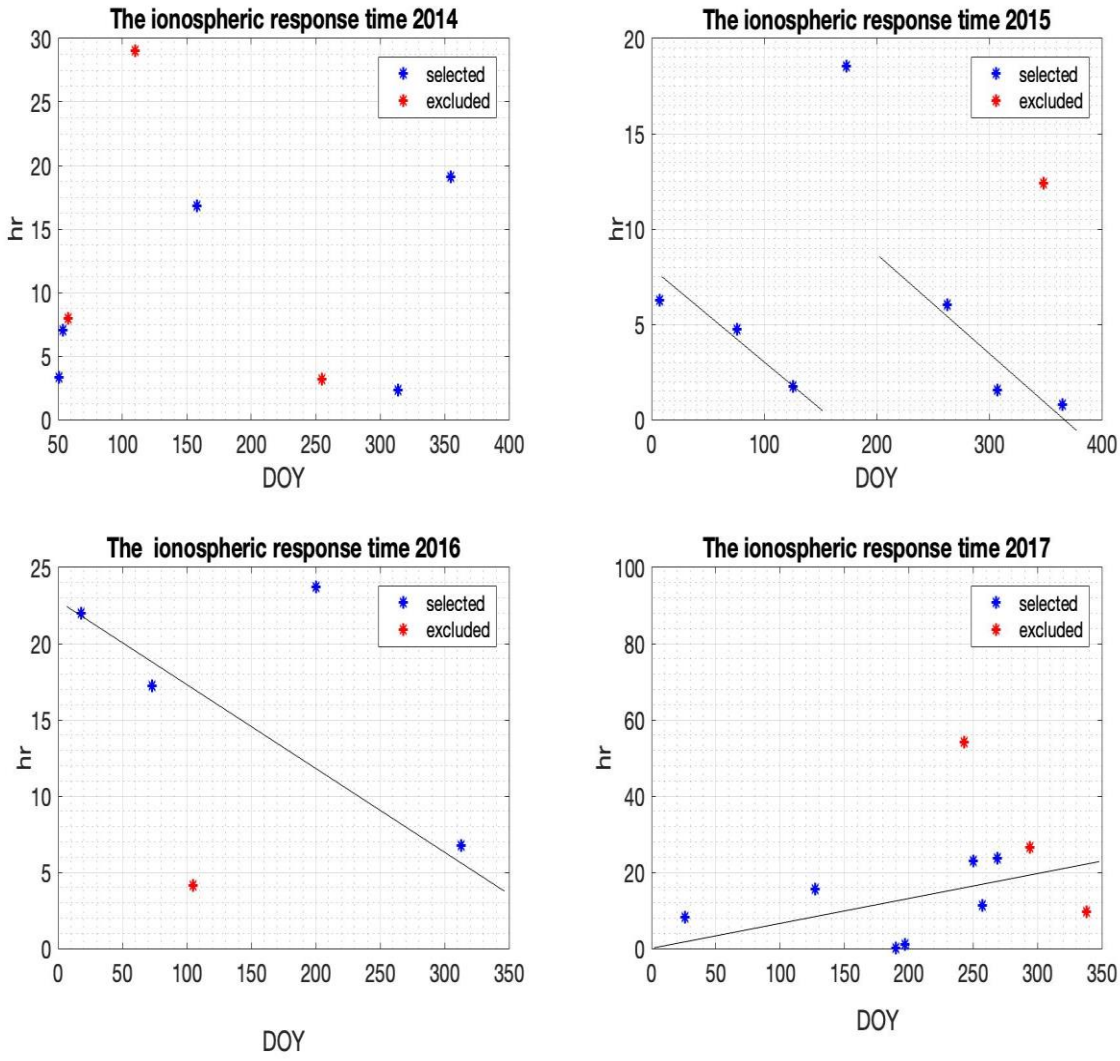
The ionospheric response time 2014
selected
excluded
hr
DOY
The ionospheric response time 2015
selected
excluded
hr
DOY
The ionospheric response time 2016
selected
excluded
hr
DOY
The ionospheric response time 2017
selected
excluded
hr
DOY

Figure 9b

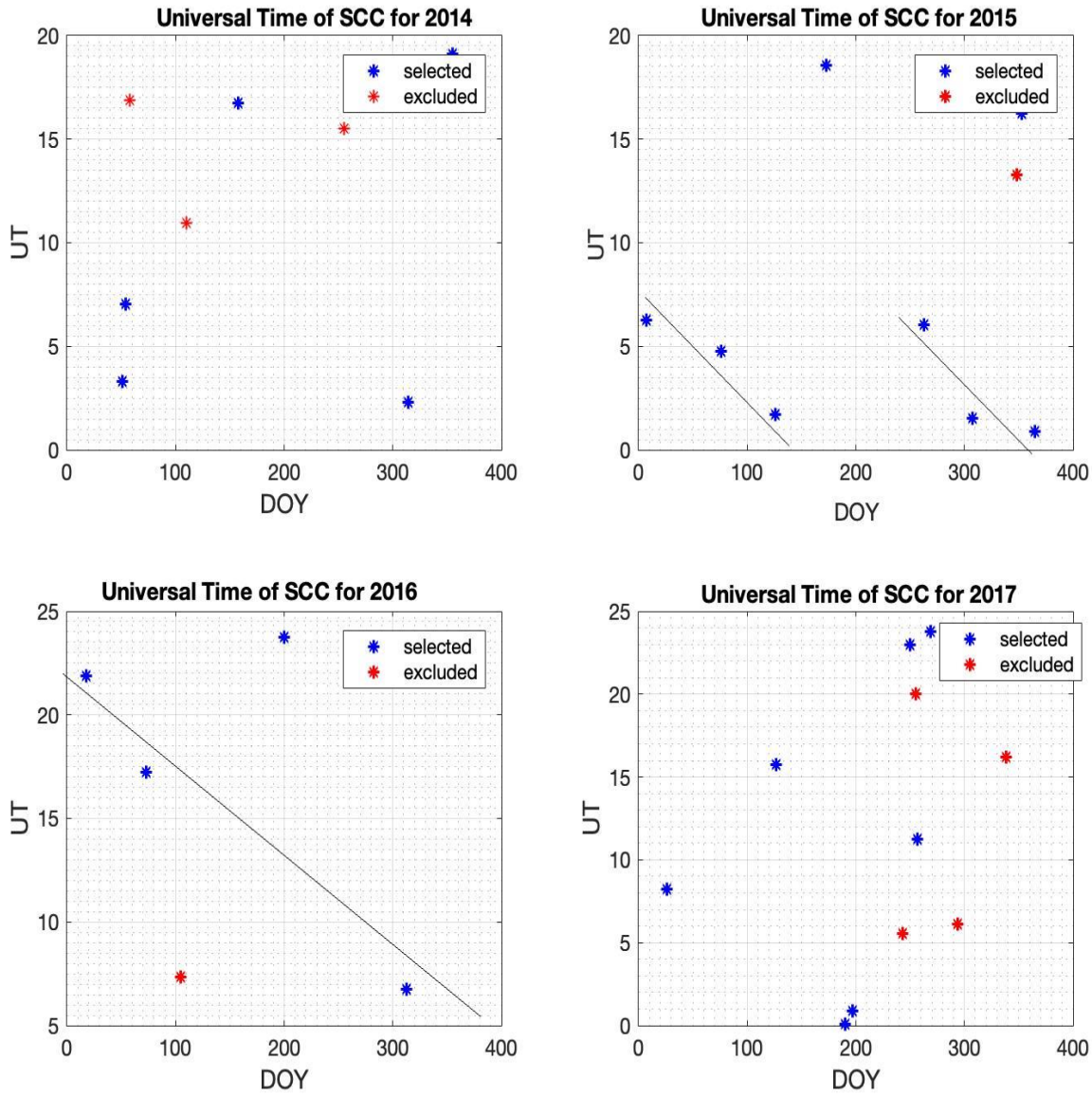
Universal Time of SCC for 2014
selected
excluded
UT
DOY
Universal Time of SCC for 2015
selected
excluded
UT
DOY
Universal Time of SCC for 2016
selected
excluded
UT
DOY
Universal Time of SCC for 2017
selected
excluded
UT
DOY